12-2018

Understanding Early Diagenetic Silicification: Petrographic Fabrics within Proterozoic Microfossiliferous Chert

Jeremy Ian Dunham
University of Tennessee, jdunham5@vols.utk.edu

To the Graduate Council:

I am submitting herewith a thesis written by Jeremy Ian Dunham entitled "Understanding Early Diagenetic Silicification: Petrographic Fabrics within Proterozoic Microfossiliferous Chert." I have examined the final electronic copy of this thesis for form and content and recommend that it be accepted in partial fulfillment of the requirements for the degree of Master of Science, with a major in Geology.

Linda C. Kah, Major Professor

We have read this thesis and recommend its acceptance:

Christopher Fedo, Molly McCanta

Accepted for the Council:
Dixie L. Thompson

Vice Provost and Dean of the Graduate School

(Original signatures are on file with official student records.)

Understanding Early Diagenetic Silicification: Petrographic Fabrics within Proterozoic Microfossiliferous Chert

A Thesis Presented for the
Master of Science
Degree
The University of Tennessee, Knoxville

Jeremy Ian Dunham
December 2018

ACKNOWLEDGEMENTS

I must first give thanks to my mother and grandfather, for whom none of this would ever have been possible. Thank you for your endless support, no matter how dark things may have gotten, you always provided the spark to keep moving forward. To my daughter who is the light of my life, and gives me the hope and inspiration I have needed to continue my efforts each and every day. I would also like to thank my colleagues in the Kah lab group who offered their support and advice throughout this process. Thank you to the many other people who have made this journey possible, and through it helped me find the gratitude every aspect of my life especially when I myself could not see it.

I would also like to thank Dr. Robert W. Rex (Scripps Institute of Oceanography) and the Lewis and Clark Fund for Exploration and Field Research in Astrobiology (American Philosophical Society), whose generous support allowed for invaluable fieldwork and sample collection. Additional support for this research and its presentation at conferences was provided by the Kenneth Walker Faculty Endowment (to LCK), the University of Tennessee Department of Earth and Planetary Sciences, and the Southeastern Section of the Geological Society of America.

ABSTRACT

Early diagenetic chert is abundant in Proterozoic carbonate successions and provides a critical window into organic preservation; the depositional origin of this chert, however, remains uncertain. There have been relatively few detailed petrographic analyses of Proterozoic microfossiliferous chert, which limits our understanding of both primary depositional fabrics, and of petrographic change during post-depositional recrystallization. The ~1.1 Ga Angmaat Formation, northern Baffin Island, Canada, contains abundant early diagenetic chert that contains exquisitely preserved microbial assemblages. Petrographic analysis indicates that chert is composed of four primary phases: chalcedony spherules that replace the majority of primary microbial and sedimentary elements, equigranular microcrystalline quartz which occurs as a minor component in the groundmass, chalcedony that lines primary voids within the depositional fabric, and megaquartz that occurs within chalcedony-lined voids. Here we present a detailed petrographic characterization of chert within the Angmaat Formation to better understand the mechanism of formation and potential pathway of diagenesis. Observations suggest that the silicification process began with formation of a silica gel within benthic microbial mats and associated carbonate sediment. We suggest that gel formation was intimately associated with the presence of organic matter (e.g., microbes and associated EPS), and that constructional voids (e.g., gas bubbles) within the mat remained free of silica gel. Polymeric linkages within the gel phase appear to have provided sufficient structure for precipitation of spherules as opal-CT, rather than as

opal-A, thus resulting in minimal water loss associated with post-depositional recrystallization to chalcedony which favored exquisite microfossil preservation.

TABLE OF CONTENTS

LIST OF FIGURES

CHAPTER ONE: INTRODUCTION

Chert is a chemically precipitated sedimentary rock predominately composed of ≥95% silicon dioxide (SiO_2), colloquially known as silica (Hesse, 1988; 1989). At Earth surface conditions, chert occurs as both a primary precipitate, such as in agates and associated void-filling cements (Graetsch et al., 1985; Lee, 2005), and as a replacement phase where silica replaces preexisting mineral phases, such as calcite, dolomite, and gypsum (Wilson, 1966; Knauth, 1979; Milliken, 1979; Clayton, 1986; Maliva et al., 2005).

Ideally, hydrated amorphous silica (opal-A) precipitates from natural aqueous solutions either abiotically, in highly silica-saturated environments, or biotically by a combination of active or passive silica sequestration processes (Folk and Pittman, 1971; Iler, 1979; Heaney, 1993; Cady et al., 1996; Lee, 2005). Low-temperature opal-A, commonly referred to as opal-AG (gel-like; Langer and Flörke, 1974; Lee, 2005), consists of similarly sized clusters of silica microspheres (1-8 μm in diameter; Lynne and Campbell, 2004). Opal-A is also distinguished by a higher disorder, and abundant stacking faults (Lee, 2005). During diagenesis, siliceous deposits undergo loss of structural water (Iler, 1979; Siever, 1962; Flörke et al., 1991; Cady et al., 1996), resulting in successive mineralogical changes from non-crystalline opal-A (or opal AG), to pseudo-crystalline opal-CT and opal-C, and finally to microcrystalline quartz (Leo and Barghoorn, 1976; Iler, 1979; Williams et al., 1985; Hesse, 1989; Flörke et al., 1991; Heaney, 1993; Cady et al., 1996; Lynne and Campbell, 2004; Lee, 2005). Opal-CT (cristobalite and tridymite) and opal-C (cristobalite) differ from opal-A in that individual

microspheres begin to show ordering, resulting in pseudo-crystalline forms that are more thermodynamically stable than opal-A. Opal-C represents the most structured and, therefore, the most crystalline of the opal varieties (Graetsch, 1994; Lee, 2005). The transition from opal-A to opal-CT has been well documented (Flörke et al., 1991; Graetsch, 1994; Lee, 2005) and proceeds by successive conversion of tridymite (30–50% in opal-CT; Graetsch, 1994) into the more crystalline form, cristobalite (opal-C). This progressive transformation of silica has been observed in both surficial sinter deposits (Lynne and Campbell, 2004; Campbell et al., 2001), where silica is a primary precipitate and transformation is associated with the age of the deposit, and in siliceous marine sediments (e.g., Murata and Nakata, 1974; Oehler, 1975; Williams et al., 1985), where transformation is generally attributed to shallow to intermediate burial (Williams et al, 1985; Simonson, 1985; Maliva et al., 1989; Hesse, 1988, 1989). A complete list of silica forms and their properties can be found in the appendix 1: Summary of nomenclature and characteristics of non-crystalline and micro-crystalline silica (Flörke et al., 1991 and Lee, 2005).

Differences between polymorphs result in optically and chemically distinct properties, such as changes in crystallographic origination and crystal habit that are recognizable in the petrographic fabric. Detailed analysis of the petrographic structure of silica phases may therefore provide information on the environmental conditions and mechanism of chert formation (cf. Wilson, 1966; Milliken, 1979; Maliva, 1985; Simonson, 1985; Hesse, 1989; Schubel and Simonson, 1990). However, there has been little comprehensive analysis of chert fabrics within microfossiliferous Proterozoic chert.

Proterozoic chert is significant as it has no discrete analogue to describe its formation. In the absence of silica sequestering organisms, it is likely that Proterozoic chert formed in a fundamentally different manner than chert in modern environments (Maliva et al., 1989). This project will provide a detailed petrographic analysis for microfossiliferous chert from the Mesoproterozoic Angmaat Formation to better understand the mechanisms of early diagenetic silicification.

Angmaat Formation chert contains exquisite preservation of depositional fabrics, including carbonate, gypsum, and halite mineral phases; microfossil assemblages; and constructional void space (Kah and Knoll, 1996; Knoll et al., 2013; Manning-Berg and Kah, 2017). The complexity of primary structures preserved within the chert are mirrored in the complexity of petrographic fabrics that comprise the chert. These include: megaquartz, equigranular microcrystalline quartz, wall-lining chalcedony (described in previous works as a likely blend of length-slow, length-fast, and moganite fibers; Graetsch et al. 1987; Heaney, 1993), and a length-fast spherulitic chalcedony phase. The presence of precursor phases and exquisitely preserved microbial elements demand chert formation to have occurred early during diagenesis from ambient fluids in surficial environments (Manning-Berg and Kah, 2017). Here we explore the fabric and composition of petrographic fabrics to better understand the process of silicification, and to aid in distinguishing the extent and pathways of post-depositional recrystallization.

CHAPTER TWO: GEOLOGIC FRAMEWORK

2.1 Bylot Supergroup

The Bylot Supergroup (Fig. 1) is a nearly 6 km thick succession of unmetamorphosed and undeformed late Mesoproterozoic sedimentary strata that is exposed within the Borden basins of northernmost Baffin and Bylot Islands, Nunavut, Canada (Kah, 1997; Kah et al., 1999; Kah et al., 2001; Turner, 2009). Within the Bylot Supergroup, three stratigraphic groups are present—the Eqalulik Group, the Uluksan Group, and the Nunatsiaq Group—that reflect the overall development of the basin (Fig. 2). At the base of the Eqalulik Group lies eruptive tholeiitic basalt flows of the Nauyat Formation which mark initial rifting of the basin (Jackson and Ianelli, 1981). Overlying this basalt is a westward-deepening, fining-upward succession of fluvial to shallow-marine quartz arenite, marine shale, and minor carbonate of the Adams Sound, and Arctic Bay formations (Turner, 2009). The carbonate-dominated Uluksan Group conformably overlies marine shale and carbonate of the upper Eqalulik Group. The lower Uluksan Group consists of lithologically homogeneous, thinly laminated microbialite facies of the Nanisivik Formation (Turner, 2009) west of a stratigraphically extensive oolitic shoal complex. This oolitic shoal marks the western edge of the Angmaat Formation, which consists of a heterogeneous package of microbial laminae, seafloor precipitates, and minor evaporite minerals (Kah, 1997; Kah, 2000) that are locally interfingered with coarse-grained siliciclastic rocks of the Fabricious Fjord Formation (Jackson and Iannelli, 1981). The lower Uluksan Group is then overlain, with a local unconformity, by subtidal carbonate platform and reef development of the Victor Bay

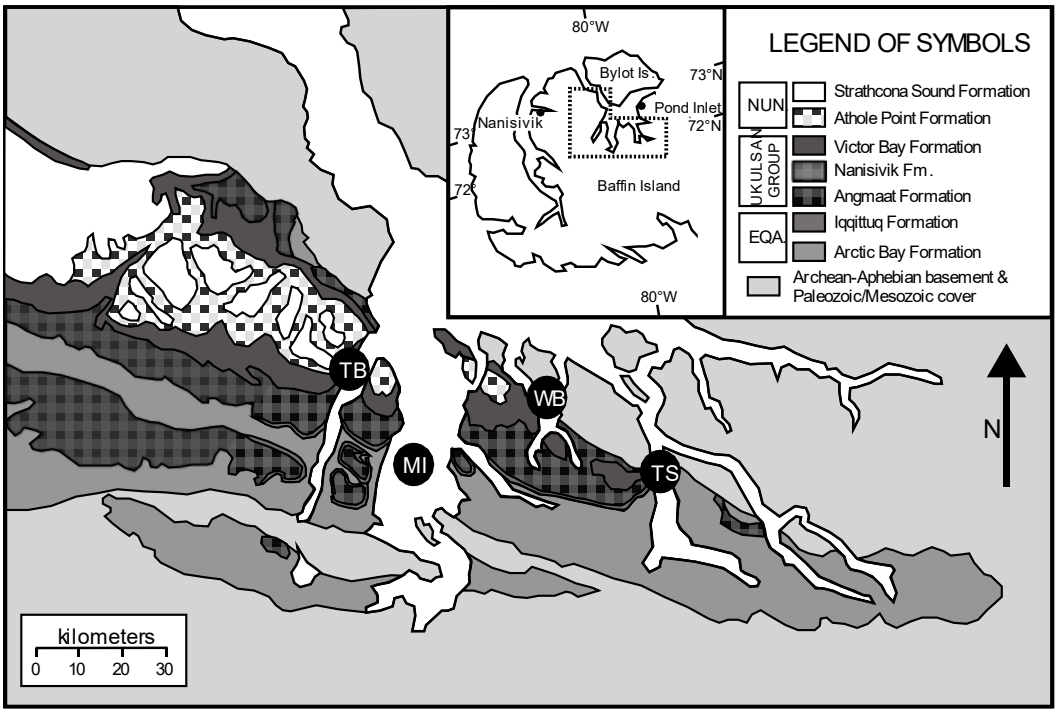

Fig. 1: Simplified geologic map of the Angmaat Formation, Bylot Supergroup (modified after Kah et al., 1999 and Knoll et al., 2013). The Angmaat Formation crops out on northern Baffin Island east of Tremblay Sound (TB). The region between Tremblay Sound and Mile Inlet (MI) represents a persistent oolitic shoal that periodically restricted eastward regions of the Angmaat Formation and allowed extensive evaporation. Chert examined for this study occurs in restricted peritidal deposits in the region between White Bay (WB) and Tay Sound (TS).

Formation (James and Narbonne, 1998; Sherman et al., 2001), and by fluvial to marine siliciclastic strata of the Nunatsiaq Group (Turner, 2009) composed of the Athole Point Formation, Strathcona Sound Formation, and the Elwin subgroup (Gibson et al. 2017).

2.2 Age Constraints

The Bylot Supergroup is broadly constrained by radiometric ages on basalt. Tholeiitic flows near the base of the Bylot succession are used to provide a maximum depositional age of 1.270 0± 0.004 Ga (U-Pb baddeleyite; LeCheminant and Heaman, 1989), and Franklinian-aged dikes that cut the entire succession provide a minimum age

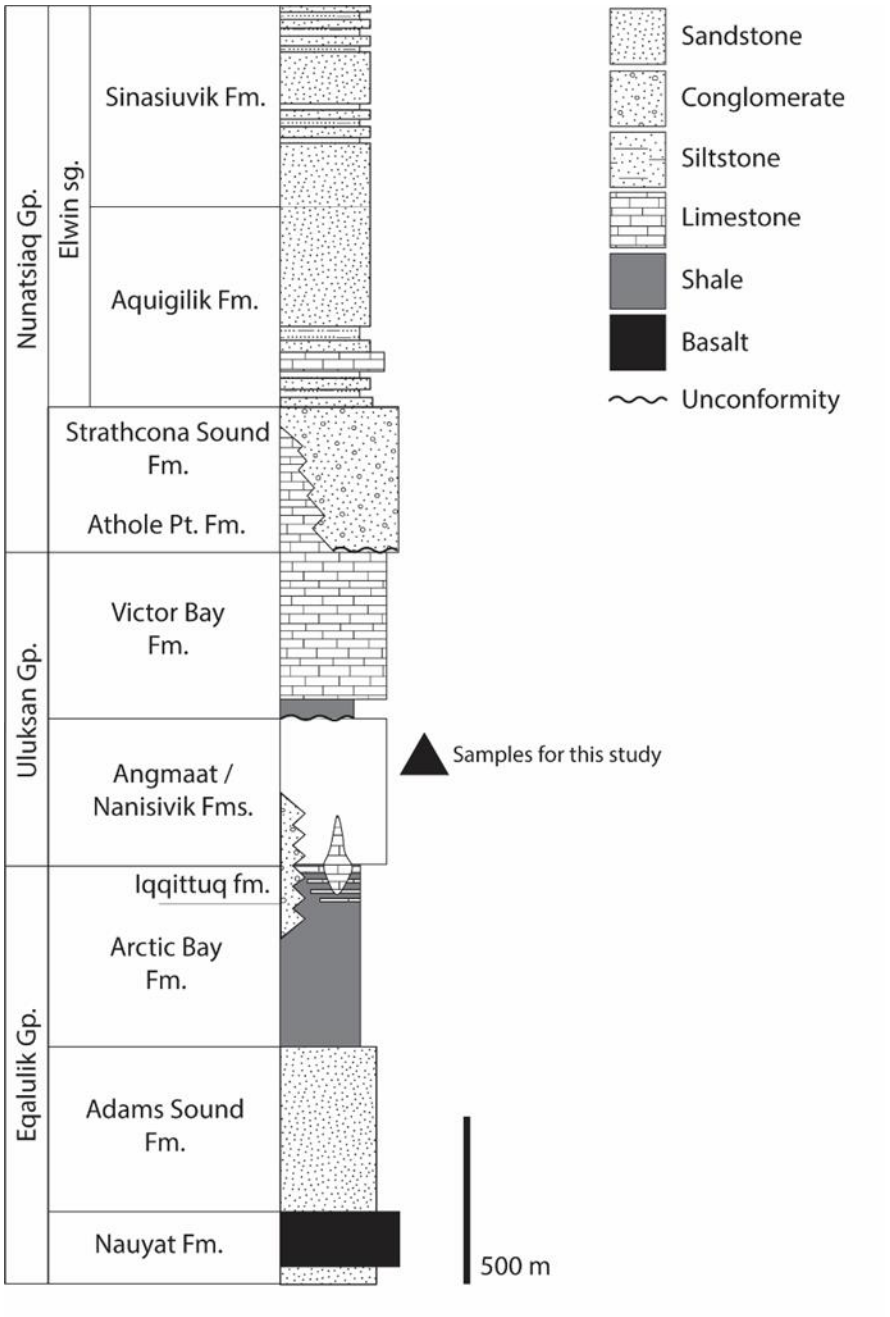

Fig. 2: Stratigraphic column of the Bylot Supergroup, modified from Gibson et al. (2017) and Turner (2009).

of ~723 Ma (U-Pb baddeleyite; Pehrsson and Buchan, 1999). Micropaleontological data from the Uluksan Group (Hofmann and Jackson, 1991, 1994) suggest that deposition of carbonate strata occurred primarily within the Mesoproterozoic. A late Mesoproterozoic age is consistent with carbon isotope stratigraphy for Uluksan Group strata (Kah et al., 1999; Kah et al., 2012), and is supported by recent geochronological data which included whole rock U-Th-Pb data from the uppermost strata of the Eqalulik Group (1092 ± 59 Ma; Turner and Kamber, 2012), and Re-Os data from black shale of the Arctic Bay Formation from the upper Eqalulik Group (1.051 ± 0.031 Ga; Gibson et al., 2017), and lowermost Victor Bay Formation (1.047 ± 0.032 Ga; Gibson et al., 2017).

2.3 Chert-Bearing Facies

In the Bylot Supergroup, chert is most abundant within the Uluksan Group, specifically within the Angmaat Formation (Jackson and Iannelli, 1981; Kah and Knoll, 1996; Hofmann and Jackson, 2001; Turner, 2009; Knoll et al., 2013). As noted previously, the Angmaat Formation (formerly the informal upper Society Cliffs Formation; Kah, 1997; 2000; Kah et al., 1999; 2001) consists of a heterogeneous package of peritidal carbonate and evaporite facies east of an oolitic shoal complex (Kah et al., 1999; Kah, 2000; Turner, 2009). Black chert (Fig. 3a) within the Angmaat Formation presents as mm-scale to cm-scale lenses and nodules, as well as semi-continuous beds (Manning-Berg and Kah, 2017). Nodules and beds are typically conformable to bedding, and reflect the morphology of primary sedimentary textures. Black chert is commonly associated with microbial facies, including stratiform microbial laminae, tufted microbial mats, and small domal stromatolites which are rarely associated with isopachously laminated seafloor

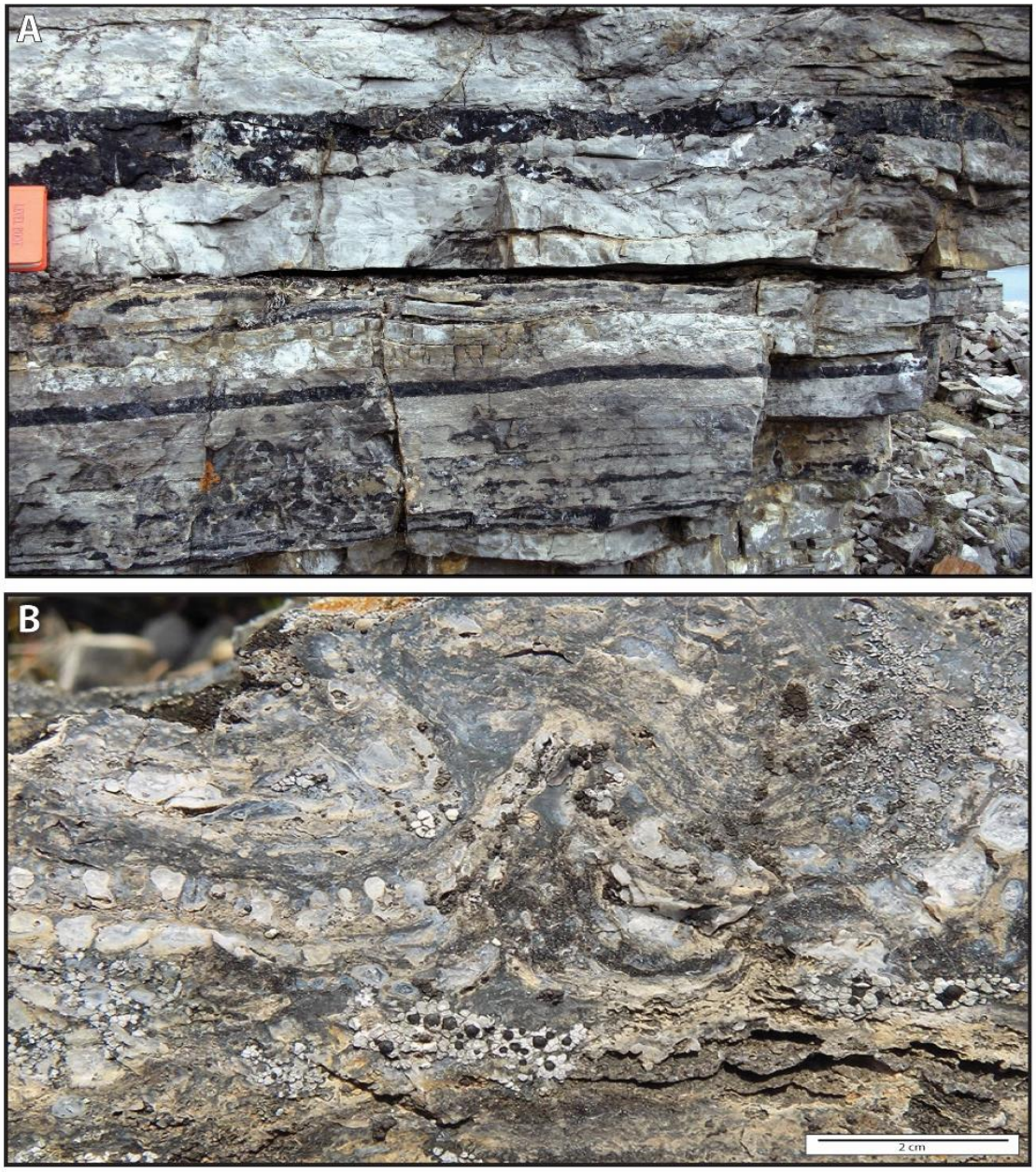

Fig. 3: Outcrop photos of microfossiliferous chert of the Angmaat Formation from near White Bay. A) Black chert occurs predominantly as centimeter-thick to decimeter-thick nodules and beds conformable with bedding. B) Tufted mat showing vertical regions of black chert that represent mat tufts, and white chert that represents chalcedony filled voids.

precipitate facies. Tufted microbial mats, in particular, are commonly observed to have an alternation of black-and-white chert (Fig. 3b) that reflects a combination of silicification of microbial elements by black chert, and infilling of primary void space by white or translucent chert (cf. Knoll et al., 2013; Manning-Berg and Kah, 2017).

CHAPTER THREE: METHODS

3.1 Optical Microscopy

In order to determine the range of microfabrics contained within Angmaat chert, detailed petrographic analysis was completed using traditional light microscopy and scanning electron microscopy (SEM). Traditional light microscopy was performed at the University of Tennessee on an Olympus BX60 compound optical microscope with a Q-imaging color camera. Observations were made using plane polarized light, polarized light, and a 550 nm gypsum retardation plate. Average crystal sizes were measured optically, using an eyepiece micrometer, and detailed crystal sizes were measured using static images and NIH Image J processing software (https://imagej.nih.gov/ij/).

3.2 Scanning Electron Microscopy

Following petrographic analysis, SEM was performed on a combination of broken rock samples and etched chips. Samples for SEM analysis were obtained by cutting mm-thick slabs from billets that were used to make thin sections, and polishing these to a 1 μm finish. By using the billets created for the original thin-sections, we were able to target specific regions observed in thin-section for SEM observation. For un-etched samples, small flakes (<1 mm^2) were chipped off from polished slabs using needle-nose pliers. For etched samples, small portions (< 5 mm^2) of polished slabs were submerged in a bath of unbuffered 48 to 50% HF solution for 15 seconds. SEM imaging was then carried out at the University of Tennessee using a PHENOM ProX (Department of Materials Science and Engineering, University of Tennessee) and PHENOM XL (Earth and Planetary Sciences, University of Tennessee), run at a constant voltage of 15 KeV for imaging. Spot analyses of chemical composition were performed using an energy-

dispersive spectrometer (EDS) in variable pressure mode (low-vacuum), and increased to 20 KeV for elemental mapping under high vacuum.

CHAPTER FOUR: PETROGRAPHIC ANALYSIS

4.1 Silicified Mat Fabrics

4.1.1 Observations. —

Previous investigations of Angmaat chert have focused on the primary depositional components that are mimetically preserved within early diagenetic chert (Hofmann and Jackson, 1991; Kah and Knoll, 1996; Knoll et al., 2013). These depositional components include filamentous and coccoidal mat structures (Hofmann and Jackson, 1991; Kah and Knoll, 1996; Knoll et al., 2013), laminae that consist of a combination of detrital carbonate and ripped-up fragments of microbial mat (Knoll et al., 2013), microlaminated seafloor precipitates (Kah and Knoll, 1996; Kah et al., 2001; Knoll et al. 2013), and preservation of evaporitic mineral phases (Fig. 4) (Kah et al., 2001; Manning-Berg and Kah, 2017).

Exquisite preservation of benthic microbial mats is the most notable aspect of Angmaat chert. Filamentous bacteria comprise the dominant microbiota preserved in early diagenetic chert. Filamentous mats consist of tightly woven filament sheaths of *Siphonophycus sp.* embedded and interlaminated with, sheaths of *Eomicrocoleus sp.* (Knoll et al., 2013). Filamentous mats occur as both undulating mm-scale laminated mats and as tufted mats that contain primary, constructional void space (Knoll et al., 2013). Little detrital material occurs within well-laminated mats, except for occasional micritic drapes and lamina consisting of ripped-up mat components.

Coccoidal mats commonly consist of a matrix of filamentous sheaths of *Siphonophycus sp.,* with local concentrations of coccoids, primarily *Glococapsa sp.*, *Myxococcoides sp*., and *Gloeodiniopsis sp.* (Knoll et al., 2013; Manning-Berg et al., in

Fig. 4: Silicified mat fabrics A) Silicified filament-dominated microbial mat consist of tightly woven filament sheaths of Siphonophycus sp. embedded and interlaminated with, sheaths of Eomicrocoleus sp. (Knoll et al., 2013). Filamentous mats occur as both undulating mm-scale laminated mats and as tufted mats that contain primary, constructional void space (Knoll et al., 2013). B) Silicified coccoid-dominated microbial mat commonly consist of a matrix of filamentous sheaths with local concentrations of coccoids, primarily Glococapsa sp., Myxococcoides sp., and Gloeodiniopsis sp. (Knoll et al., 2013; Manning-Berg et al., in prep). Billowy, darker stained regions that are interpreted extracellular polymeric substances (EPS) (Knoll et al., 2013). C) Silicified, mimetically-replaced aragonite fan which occur as seafloor precipitates.

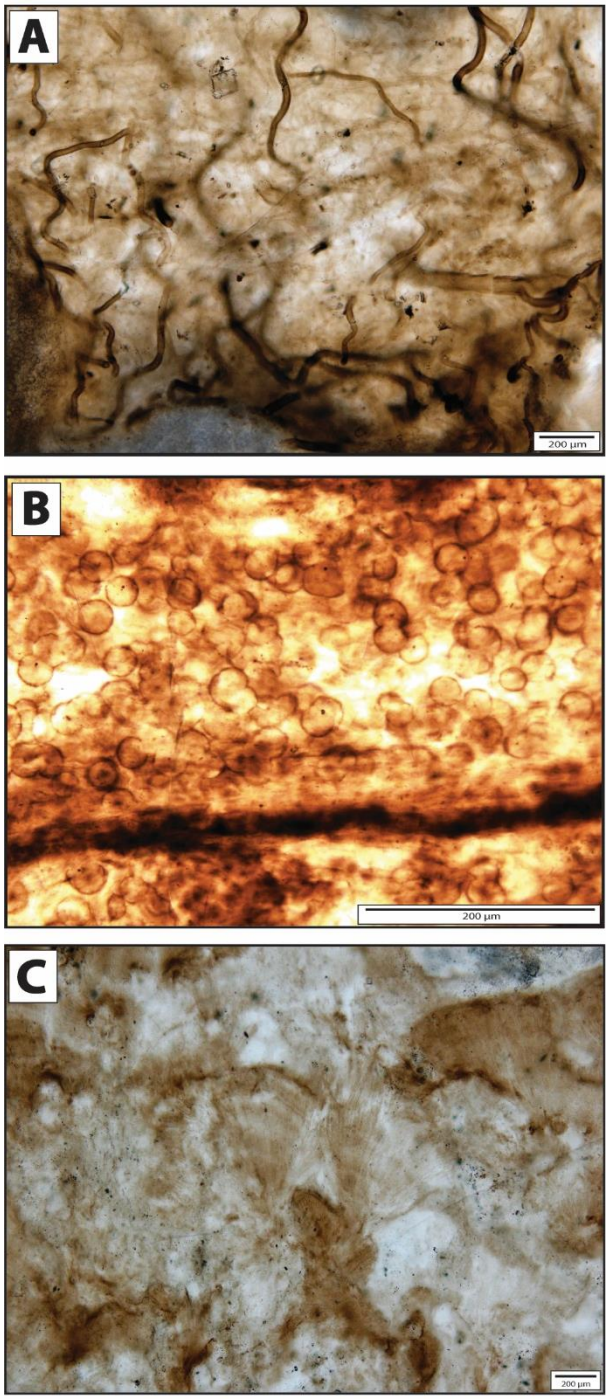

Fig. 4: (Continued)

prep). More rarely, coccoidal mats dominated by *Eoentophysalis sp.*(Knoll et al., 2013) are associated with µm-scale laminated precipitates, and detrital breccias (Kah and Knoll, 1996; Knoll et al., 2013). Coccoid-rich mats, in general, contain billowy, organically stained regions that are interpreted extracellular polymeric substances (EPS) (Knoll et al., 2013).

4.1.2 Interpretations. —

Angmaat Formation chert records spectacular preservation of primary benthic (deep-water) constituents, including an array of microbial mat fabrics, substrate voids, and seafloor precipitates. Fabric retentive replacement, or mimetic preservation, is often defined as when a primary mineral phase is preserved within a secondary mineral phase without alteration of its primary morphology (e.g., mimetic fabrics in dolomite, Sibley 1991). In the case of the Angmaat chert, silica mimetically preserves both organic constituents (e.g., mat structures; Knoll et al., 2013), in which case the silica actually represents precipitation of a primary mineral phase, and primary mineral features (e.g., seafloor precipitates and evaporite minerals; Kah and Knoll 1996; Kah, 2000; Kah et al. 2001; Knoll et al., 2013), where silica represents a secondary mineral phase.

The exquisite preservation of microbial elements, which commonly decay in a matter of days (cf. Bartley 1996) indicate that silicification must have occurred penecontemporaneously with deposition. The mimetic preservation of primary mineral phases (e.g., aragonite, gypsum, and halite) further indicate that silicification likely occurred under a range of elevated saturation states, and proceeded via fluctuations in pH

(Manning-Berg and Kah, 2017) or changes in mineral solubility associated with growth of the secondary crystals (Maliva et al., 2005).

4.2 Void-Filling Chert Phases

4.2.1 Observation. —

Two discrete modes of silicification are present within Angmaat chert voids, similar to that of agate systems, which commonly contain a succession of wall-lining chalcedony followed by a megacrystalline quartz (megaquartz) phase (cf. Graetsch et al., 1985; Lee, 2005). Void boundaries are marked by an abrupt transition to microfossiliferous chert (Fig. 5; cf. Knoll et al., 2013). Occasionally, voids contain a lower (geopetal) fill of non-silicified carbonate, before precipitation of the chalcedony phase.

Void-filling chalcedony does not contain any clear evidence of mineral inclusions, although in plane-polarized light void-filling chalcedony commonly shows variation in color that presents as either an overall light brown staining of acicular fibers, or as multiple, discrete, isopachous color bands. Void-lining chalcedony occurs predominantly as length-fast orientation (observed with the addition of the gypsum plate), but occasionally also contains secondary events of both length-fast and length-slow chalcedony.

In smaller (sub-mm) voids, chalcedony is commonly the only void-filling phase. In larger voids, however, chalcedony is followed by megaquartz, which occurs as the terminal phase within the center of the voids. Megaquartz is composed of relatively large (<2mm) equant crystals, that display pin-point extinction. In the largest voids, megaquartz grains appears to coarsen from the fringe of the wall-lining chalcedony

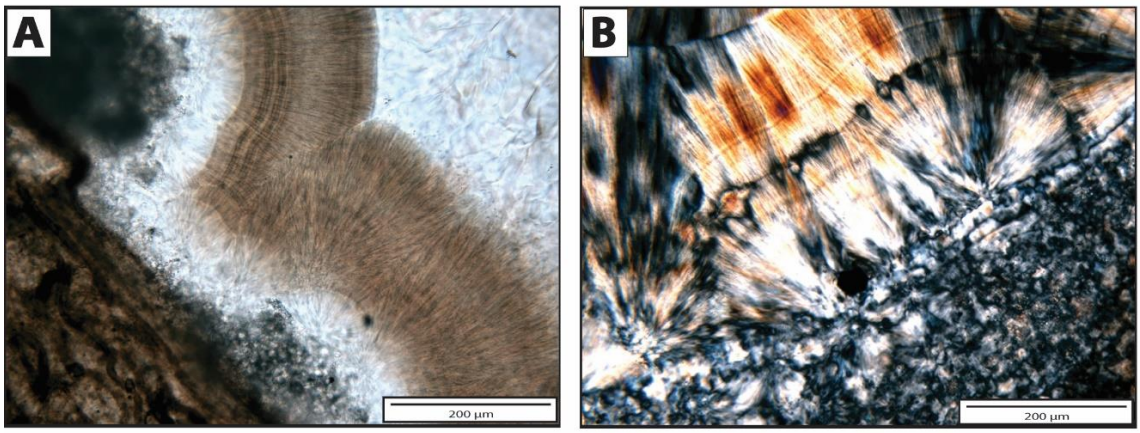

Fig. 5: Images of a mm-scale void within microfossiliferous Angmaat Formation chert. Voids are recognized by the progression from banded wall-lining chalcedony and filled by equigranular megaquartz. A) Plane-polarized image which displays a successive transition darkly-banded, wall-lining chalcedony, to megaquartz. The wall matrix material of densely-woven filamentous mat, evidenced by very-fine crystals near the rim of the void is also preserved. B) Cross-polarized image of mm-scale void which displays banding which appears within discrete episodes of cement formation (i.e., syntaxial growth), and two chemically distinct episodes of banding (evidenced by gypsum plate as length-fast, followed by length-slow chalcedony).

toward the center of the void, however this is difficult to distinguish in most of the smaller voids. This grain coarsening appears distinct from coarsening events attributed to Oswald ripening.

4.2.2 Interpretations. —

Millimeter-scale voids occur within Angmaat formation chert and are interpreted as constructional within microbial mats that result from gas-filled pockets produced as a consequence of microbial metabolic activity (Knoll et al., 2013). The absence of carbonate inclusions within the silica phases in these voids suggests that silica is a primary mineral phase, rather than the mimetic replacement of a precursor carbonate phase (Maliva et al., 2005).

The presence of a succession from void-lining chalcedony to megaquartz suggests the presence of fluid-filled voids, in which silica concentration decreases through time as silica is consumed (cf. Folk and Pittman, 1971; Heaney, 1993; Lee, 2005). Nucleation occurs at margins of the voids potentially catalyzed by the presence of surface-charged organic materials. Elevated silica saturation then favors crystallization with a fibrous growth habit (Heaney, 1993; Lee, 2005). When silica concentration is depleted by continued chalcedony growth, crystallization of megaquartz ensues as it is thermodynamically favored to precipitate over other silica phases at low silica saturation states (Hesse, 1989; Heaney, 1993).

Color banding within chalcedony is commonly attributed to instability in crystal growth at the crystallization front resulting from the incorporation of cations, such as Al, Na, K, Fe, etc., within the crystals as they grow (Heaney, 1993; Wang and Merino, 1995; Merino et al., 1995; Lee, 2005). In the samples collected from the Angmaat Formation of northern Baffin Island, potential instability of crystal growth does not appear to be related to discrete nucleation events, associated with competitive growth, but rather to incorporation of trace elements or fine detrital constituents (e.g., clay, organic matter) into the crystal structures during syntaxial crystal growth. This suggests that the presence of banding within chalcedony can be attributed to relatively minor changes in fluid composition during crystal growth. By contrast, banding associated with re-nucleation of void-lining chalcedony commonly shows changes in fiber orientation (i.e., length-fast to length-slow), suggesting the potential for discontinuous growth and abrupt changes in fluid chemistry (Folk and Pittman, 1971; Heaney, 1993).

4.3 Microcrystalline Chert

4.3.1 Observations. —

Microcrystalline quartz comprises the majority of Angmaat Formation chert. Under cross-polarized light microcrystalline chert shows notable differences in coloration, whereby darker regions are represented by finer crystal sizes and strongly correlated with the increased density of organic staining/matter (Fig 6a and 6b).

The majority of microcrystalline quartz within Angmaat chert is composed of spherulitic chalcedony. Under low magnification and crossed-polarized light, spherulitic chalcedony is marked by the presence of wedge-shaped regions of extinction that define a regional rectilinear pattern (Fig. 6c and 6d). Under higher magnification, wedge-shaped regions more clearly define a spherical cross-section with alternating extinct and non-extinct quadrats that rotate with rotation of the stage. The addition of the gypsum plate (Fig. 7) significantly enhanced a rectilinear pattern defined by alternating regions of extinction, thereby permitting easier, and more rapid recognition.

At higher-magnification, the observed rectilinear pattern is defined by the presence of discrete units of radiating fibers from a central point, interpreted to be spherules of fibrous-radial chalcedony. Individual spherules within this fabric range between 10 µm to 200 µm in diameter; however, they generally appear to be similar sizes within discrete regions. Observation using the gypsum plate shows that rectilinear lineations reflect the consistent presence of reddish or “red” color in the NW-SE direction, and bluish or “blue” color in the NE-SW direction relative to the field of view. Retardation of light is observed in the fibers perpendicular to the direction of insertion of the gypsum plate (i.e., aligned with the slow direction of the gypsum plate), thus,

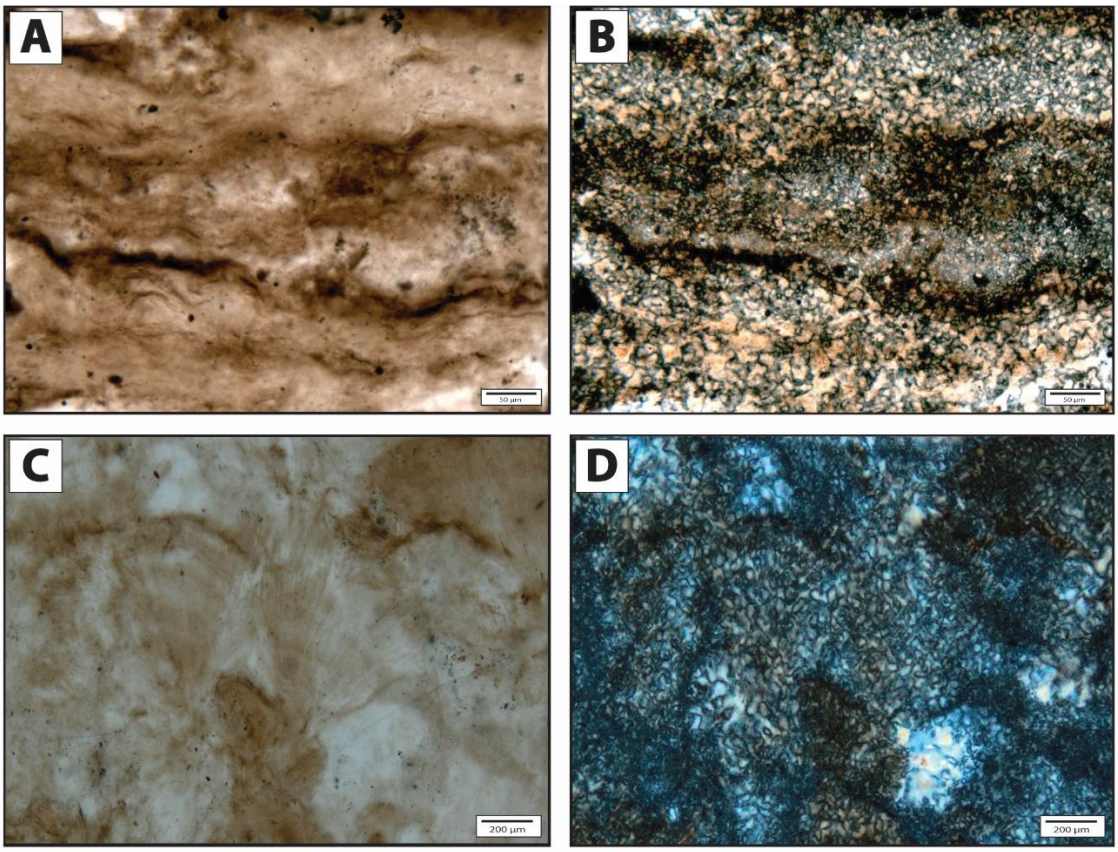

Fig. 6: Silicified microcrystalline chert fabrics, where A) Compacted filament-dominated mat showing concentrations of organic-rich, microcrystalline silica. B) Compacted filament-dominated mat under crossed-polarized showing differences in crystal size associated with organic content. Silicified, C) Mimetically-replaced aragonite fan fabric in plane-polarized light at low-power, and surrounded by dark regions indicative of organic matter/staining. D) Mimetically-replaced aragonite fan under cross-polarized light which display a rectilinear fabric can be see that is not readily visible in plane-polarized light.

indicating that these individual spherules are composed of length-fast oriented chalcedony. Differences in the angle of intersection within the rectilinear fabrics appears to reflect differences in spherule size, and potentially differences in spherule packing.

At higher magnification within discrete regions, individual spherules occur as (1) isolated spheres (Fig. 7a), separated by a more equant, granular microcrystalline quartz phase (Fig. 7b), as (2) spheres that have grown into each other and share a compromise boundary (Fig. 7c), and as (3) spheres show secondary overgrowths of chalcedony, which is often length-slow (Fig. 7d). SEM observations provide more detailed structural observations. Broken chips yielded images that show radial fibrous spheres. Where the external portions of the spheres are visible, spherules are clearly composed of individual acicular fibers (Fig. 8). Pockets of more equigranular crystal matrix (≤30 μm) are observed. HF etching reveals that the primary groundmass is composed of abutting spheres consisting of very-fine (<1 μm) radially orientated acicular crystals. When visible, the central nucleation site often is represented by a single dark point of less relief, or two smaller points side by side.

SEM analysis performed on etched samples also shows the potential relationship between organic constituents and randomly oriented slices through spherulitic chalcedony. Organic constituents are identified using SEM (Fig. 8d) as dark folded features with distinctly higher topographic relief. Although it is generally difficult to observe the relationship between microbial constituents and spherules, here the fibers of the radial spheres appear here to nucleate within the matrix of the chert, not on the

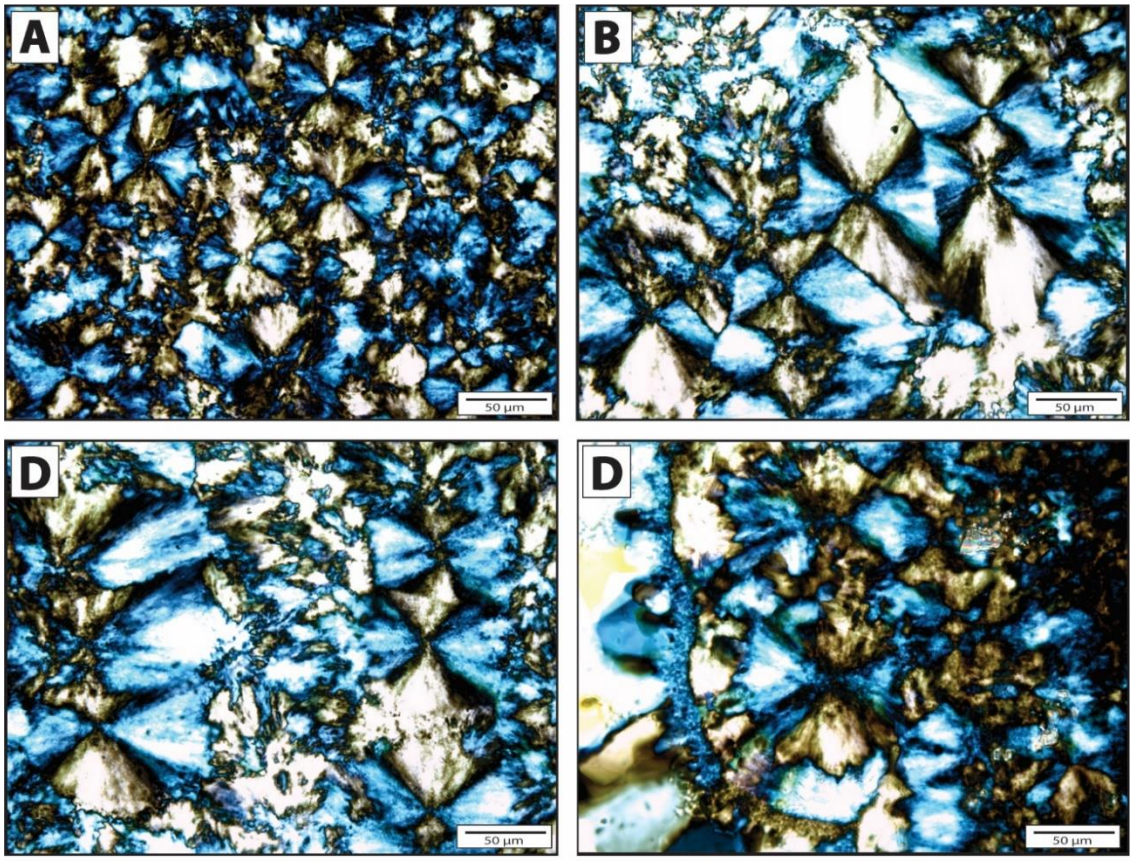

Fig. 7: Boundaries of spheres and cements at high power with the use of cross-polarized light and gypsum plate. A) Demonstrates the uninterrupted and spherulitic nature of these spheres when not touching each other. B) Shows how these spheres tend to grow into each other forming linear compromise boundaries. When space exists between these spheres there can be either C) very-fine microcrystalline cements that form with no clear orientation, or D) Syntaxial overgrowths nucleating on the surface of the preexisting spheres, which can sometimes display a shift from length-fast to length-slow orientation.

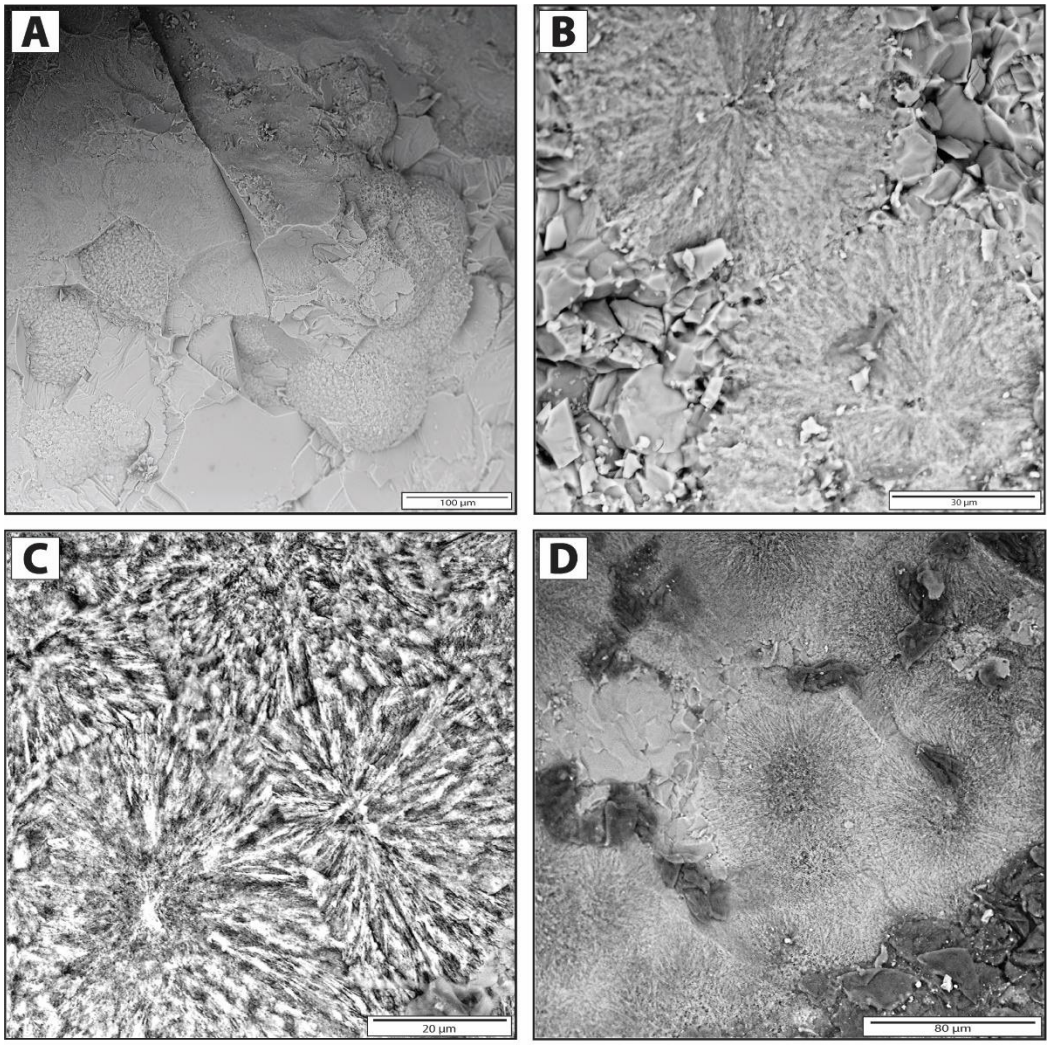

Fig. 8: SEM images of fibrous-radial spheres. A) The globular surface of these spheres. B) Displays the boundary between two fibrous-radial spheres, surrounded by a microcrystalline quartz matrix displaying the stark difference between these two fabrics, and C) HF etched surface clarifying the fibrous nature of these spheres and the boundary that exists between them. D) Show the dark, globular organic constituents present in relation to the fibrous silica spheres, however, the spheres appear to be growing outside, and permeating through the organic components as opposed to nucleating on the surfaces.

surfaces of the organic matter, and continue to grow in the same manner through the organic matter uninterrupted. These distinct spherules were abundantly distributed throughout the chert and were determined by energy-dispersive spectroscopy (EDS) analysis to be composed entirely of silica. With that said, the site of nucleation for the discrete spherules could not be seen provided the limitations in resolution, and EDS was unable to distinguish and differences in composition between the chalcedony fibers and the central pore.

Although spherulitic chalcedony is most prevalent in association with microbial mat textures, it also occurs in association with primary mineral fabrics. For instance, spherules mimetically replace primary aragonite fan fabrics. Within regions where the precursor aragonite fans were present, dense fields of very-fine crystals are present which exhibit a rectilinear to spherulitic habit (Fig 6c and 6d). However, in regions directly adjacent, crystal sizes appear larger and composed of equigranular microcrystalline quartz, determined by the presence of pin-point extinction in cross-polarized light. In addition to mimetically replaced fans, dolomite rhombs (~50 μm) randomly interspersed within the chert fabrics were also seen to be replaced by spherules.

In order to better understand the potential relationship between the density of organic staining and the size of chalcedony spherules, we performed crystal size distributions (CSDs) on chalcedony spherules in several microbial-dominated regions. CSDs are used to better understand nucleation and growth parameters in a crystalline phase (cf. Kile et al., 2000; Kile and Eberl, 2003). To perform the CSD analysis, petrographic images, using the gypsum plate for clarity, were uploaded into Image J

software. By visual inspection, three groups were defined that displayed differences in both crystal size and the density of organic staining. Within these regions, individual spheres were identified and defined as four alternating wedge-shaped regions ("red" and "blue" with the gypsum plate) that radiate from a central point, (Fig. 9); diameters were measured in both the "red" and "blue" directions. More than three thousand individual diameters were measured (Appendix) and graphed using SPSS statistics software from IBM (https://www.ibm.com/us-en/marketplace/spss-statistics).

Results of CSD measurements are shown in Fig. 10. The majority of fine-size fraction measurements ranged between 15-25 µm, averaging approximately 20 µm in diameter; medium-size fraction ranged between 25-50 µm, averaging approximately 35 µm; and coarse-size fraction measurements ranged between 40-100 µm, averaging approximately 60 µm. Though the fine-size fraction displays a slight skewness toward the right, distribution curves for all three groups are consistent with a lognormal distribution (i.e., where the primary mode is at a smaller grain size than both the mean and the median grain size).

4.3.2 Interpretations. —

Chalcedony spherules comprise the majority of microcrystalline chert phases, representing both silica deposition as a primary mineral phase within microbial mats, and as a secondary phase that mimetically replaces both aragonite fans and dolomite rhombs. Radially oriented, fibrous chalcedony spheres contrast with the equigranular microcrystalline quartz that represents only a minor percentage of the fabric, and generally occurs as cements between spherules. The ubiquity of length-fast chalcedony

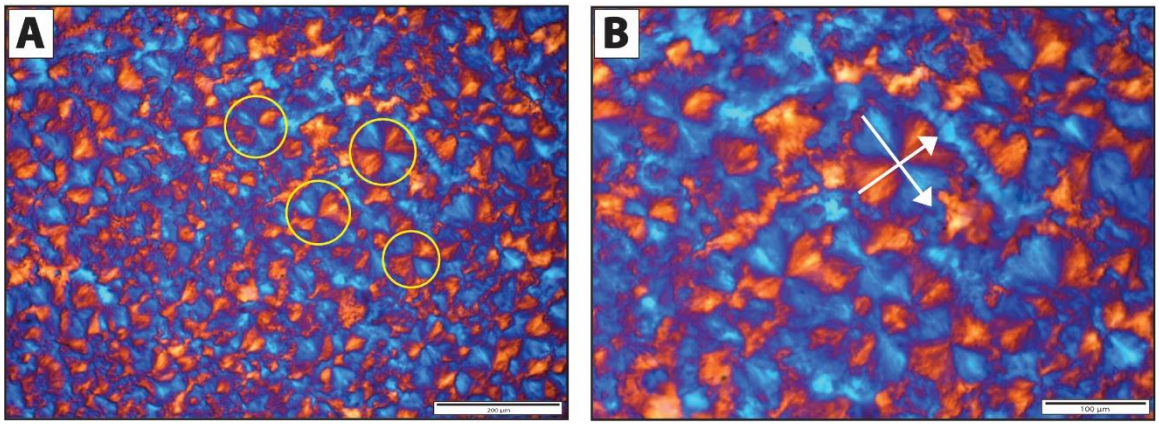

Fig. 9: A) Discrete fields with visible "red" (NW-SE) and "blue" (NE-SW) lineation were compiled for CSD analysis using the gypsum plate for clarity. B) Individual spheres were identified and defined as four alternating wedge-shaped regions ("red" and "blue" with the gypsum plate) that radiate from a central point, after which diameters were measured in both the "red" (NW-SE) and "blue" (NE-SW) directions.

spherules observed in the Angmaat chert is distinct from that observed in most Proterozoic microfossiliferous chert, which is commonly described simply as "microcrystalline quartz" (Tyler and Barghoorn, 1954; Oehler and Logan, 1977; Mendelson and Schopf, 1982; Southgate, 1986; Schopf et. al., 2008). We do note that in our original thin sections, which were cut 100 µm thick for analysis of microbial elements, the rectilinear fabric associated with chalcedony spherules were apparent only in mimetically replaced aragonite fans, where spherules are exceptionally large. This observation suggests that identification of spherules is readily impeded when section thickness exceeds spherule diameter. Nucleation and growth of spherules can be examined using measured CSDs. CSDs can be characterized as one of three basic shapes: (1) an asymptotic shape (Fig. 11a), which reflects constant-rate nucleation accompanied

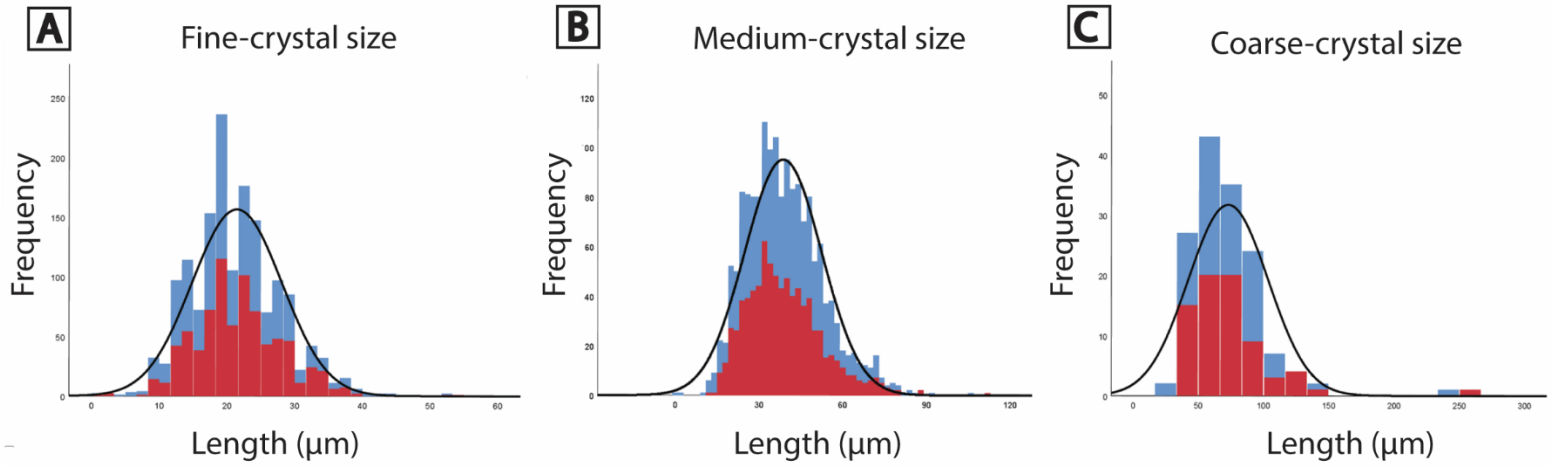

Fig. 10: Results of CSD analysis. Three graphs represent the three groups representing different ranges in crystal size. Red and Blue colors correspond to measured lineation in the north-south direction and east-west direction respectively. These measurements were compiled using SPSS statistics software and graphed as simple histogram plots for interpretation. A) Fine-size fraction measurements ranged between 15-25 µm, averaging around 20 µm in diameter (Blue- Mean=21.0567, Std. dev.= 6.71241, n=768; Red- Mean=21.8462, Std. dev.= 6.54387, n=793). B) Medium-size fraction ranged between 25-50 µm, averaging around 35 µm (Blue- Mean=38.7853, Std. dev.= 14.14307, n=829; Red- Mean=38.5332, Std. dev.= 13.45123, n=814). C) Coarse-size fraction measurements ranged between 40-100 µm, averaging around 60 µm. Though the fine-size fraction displays only a slight skewness toward the right, distribution curves for all three groups are consistent with a lognormal distribution (Blue- Mean=71.9077, Std. dev.= 29.24962, n=73; Red- Mean=73.7446, Std. dev.= 32.13461, n=73).

by crystal growth in a nutrient-limited system, where nucleation rate rapidly declines upon initial crystallization; and (3) a theoretical steady-state curve (Fig. 11c), attributed to Ostwald ripening. The model is Fig. 11c represented by a rightward shift in the mode of the lognormal curve that is attributed to growth of larger crystals at the expense of smaller crystals when saturation state of the system decreases. Ostwald ripening results in overall coarsening of the crystal fabric and homogenization of overall crystal sizes.

Crystal size distributions (CSDs) measured in the Angmaat chert show a distinct difference in crystal size between regions of different organic staining, in which the density of organic staining (here inferred to represent the density of organic molecules) is correlated to smaller spherules. This relationship between organic staining and crystal size suggests that organic matter likely played a key role in nucleation of silica spherules, however, as the spherules do not appear to be nucleating on the surfaces of the

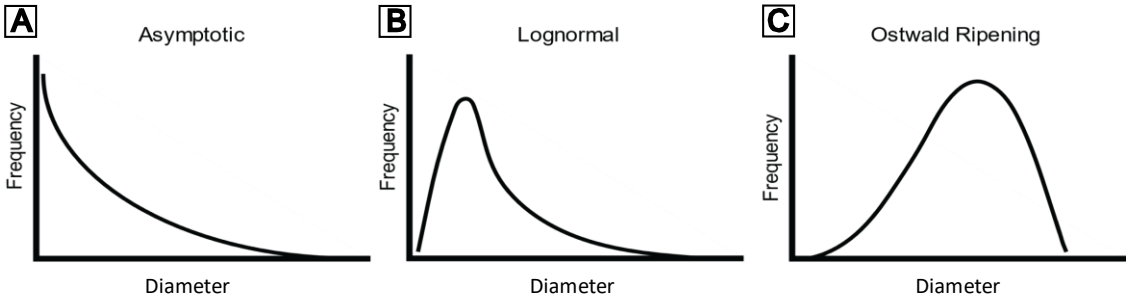

Fig. 11: Three basic shapes of Crystal Size Distributions (modified from Eberl et al., 1998; Kile et al., 2000: Kile and Eberl, 2003). A) Asymptotic curve related to constant-rate nucleation accompanied by surface-controlled growth in an open system. B) Lognormal curve which results from rapid nucleation followed by a rapid rate of decay in nucleation in a closed system. C) A theoretical, universal, steady state curve attributed to Ostwald ripening seen as a rightward shift in the curve.

microfossils the nature of this relationship is not well understood. Additionally, in each region, CSDs are dominated by smaller crystals fractions, suggesting a lognormal distribution (Fig. 11; Kile et al., 2000; Kile and Eberl, 2003). Discrete regions with the finest crystals appear to show a more normal distribution pattern, suggesting the potential of limited Ostwald ripening. A Skewness-Kurtosis test for normality, however, was performed in SPSS (Ghasemi and Zahediasl, 2012; Cramer and Howitt, 2004) and shows that each of the three regions is, in fact, statistically skewed, and therefore reflected a true lognormal distribution. The results of the Skewness-Kurtosis test for normality as calculated by SPSS were as follows: 2.814 ± 0.060 for the fine, 0.549 ± 0.060 for the medium, and 0.727 ± 0.060 for the coarse.

These lognormal distributions seen in the data in Fig. 10 suggests that crystallization was dominated by spontaneous nucleation, with limited Ostwald ripening. Decay-rate nucleation suggests that Angmaat chert represents a nucleation-dominated control on crystal size with high initial nucleation reflecting a spontaneous nucleation event. Although nucleation rate may have been facilitated by the presence of organic constituents within the benthic microbial mats (e.g., dissolved organic matter, EPS), evidence for decay-rate nucleation suggests that the nucleation process was initiated by an abrupt change in environment, such as a change in pH (Manning-Berg and Kah, 2017).

Combined, the large size of the spherules ($\leq$150 μm diameter), the presence of both discrete spherules and spherules joined at compromise boundaries, and discrete regions of different crystal size, suggest that nucleation likely occurred within a silica gel

phase (Oehler, 1976; Hattori et al., 1996). A preserved lognormal CSD further suggests that nutrient influx to the system was limited, which is consistent with precipitation of spherules by transport limited growth (cf. Cady et al., 1996) within a gel phase. Only the finest crystal size fraction shows evidence for limited Ostwald ripening, which may reflect the presence of a more water-rich, less viscous initial silica gel.

Additional evidence that spheroidal silica that replaces microbial mat fabrics precipitated within an initial gel phase comes from the differences in chalcedony growth between silicified mat phases and constructional voids. The fundamental observations to consider include (1) the presence of apparently randomly nucleated spherules throughout primary microbial mats, (2) distinct boundaries that separate regions of spherulitic chert and void-lining chalcedony, (3) distinct banding (both in coloration and fiber orientation) in void-lining chalcedony.

If both microbial mats and the constructional voids within the mat (cf. Knoll et al., 2013) were permeated by an initial silica gel, we would expect no clear distinction in crystal morphology. In this model a continuous gel matrix would favor random nucleation that would cross the original mat-void boundaries. Even if differences in the density of organic matter within the gel favored nucleation at the original mat-void boundary, the diffusion limiting structure of silica gels would favor neither the distinct sequence of mineral fabrics observed from rim to center of the void, nor the presence of banding. In an alternative scenario, the difference in organic content between the microbial mat matrix and the constructional void may have resulted in a less-polymerized gel within the void. This model might result in the potential for different fabrics at the

rim and the core of the void, but would, again, likely lack the distinctive banding found within the fibrous void-lining chalcedony.

We suggest that, even in the earliest stage of silicification, the microbial mats themselves fostered a range of environments, wherein organic acids within the mat fabrics aided in the polymerization of an initial silica gel, even as the constructional voids within the mat remained open to fluid transport. In this case, crystallization proceeded within the void space from a silica-rich fluid that was likely related to, but distinct from, the surrounding gel phase. In this scenario, crystallization initiated as acicular isopachous rims within the void space, potentially nucleated at the boundary with a silica gel phase. Within the void, fluids could change readily in composition, even as the diffusion-limiting gel retained a more homogeneous chemistry. Changes in fluid chemistry within voids then resulted in observed banding and changes in mineralogical structure of void-lining chalcedony.

Finally, with respect to microfossil preservation, limited observations suggest that chalcedony spheres nucleate and grow unperturbed by the presence of either disseminated organic matter or discrete microfossils within the matrix. Several recent investigations suggest that mineralization and preservation of microbial mats represent nucleation occurring on the charged surfaces of microbial sheaths (e.g., Konhauser, 2004; Lalonde et al., 2005; Shang et al., 2018). By contrast, here spherule nucleation shows no correlation with discrete microbial elements. Rather, chalcedony fibers appear to permeate the organic matter without disturbing its primary structure. Such observation is consistent with syntaxial spherule growth, wherein crystallites are aligned with previous

growth and readily incorporate environmental constituents as micro-inclusions (Hesse, 1987, 1989).

CHAPTER FIVE: DISCUSSION

Petrographic examination shows that early diagenetic silica within the Angmaat Formation occurs primarily as spherulitic, length-fast chalcedony. Although spherulitic chert has been previously recognized in Proterozoic chert (Maliva et al., 1989; Maliva et al., 2005), it has not been recognized as the primary diagenetic phase. In the Angmaat chert, spherulitic fabrics comprise both the primary mineral phase in the silicification of benthic microbial mats, and as a secondary mineral phase in the mimetic replacement of aragonitic seafloor precipitates. Chalcedony also occurs as the initial depositional phase within primary substrate voids.

5.1 Chalcedony Growth

Spherulitic growth is common in natural systems, predominately as length-fast chalcedony (Folk and Pittman, 1971; Hesse, 1989; Heaney, 1993). Both spherulitic and void-filling chalcedony within Angmaat Formation chert are dominantly length-fast, although length-slow chalcedony occurs as a secondary growth phase within both microbial mats and within primary void space. Typically, during crystal growth, c-axes occur parallel to the direction of fiber elongation; this orientation is known as length-slow (Fig. 12), because crystallites are stacked parallel to the c-axis, and the resulting fibers being elongated along the non-polar [0001] direction (Folk and Pittman, 1971; Frondel, 1978). By contrast, length-fast growth (Fig. 12) results from crystallites stacked perpendicularly to the c-axis, where the resulting fibers are elongated either along [1120] or, more rarely, along [1010]; fibers may also be seen as twisting around the elongation axis (Frondel, 1978).

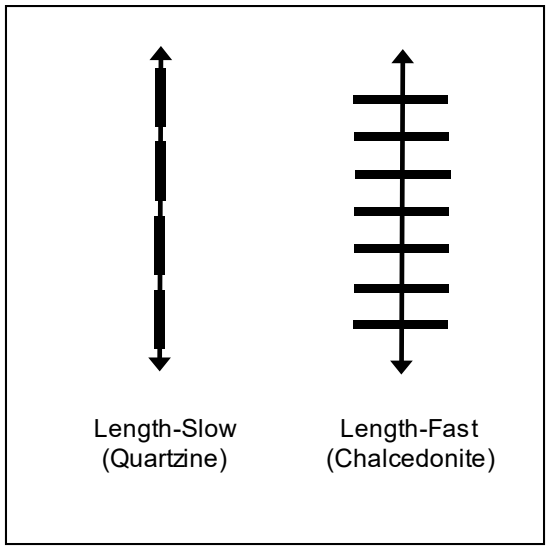

Fig. 12: Orientation of crystallites in relation to crystallographic c-axes in fibrous silica minerals (modified after Milliken, 1979 and Hesse, 1989). A) Crystallites are oriented parallel to crystallographic c-axis implying length-fast orientation. B) Crystallites are oriented perpendicular to crystallographic c-axis implying length-fast orientation.

In silica systems, differences in crystal form result from influence of pH on crystallization (Folk and Pittman, 1971; Iler, 1979; Heaney, 1993). At elevated pH (i.e., values greater than 7), silica becomes ionized and forms discrete silica tetrahedra [SiO_4], which attach themselves to the growing surface (Fig. 13b), and result in fibers with their c-axes parallel to the direction of fiber elongation (i.e., length-slow orientation; Folk and Pittman, 1971; Hesse, 1989). However, at lower pH (i.e., values less than 7) and at high silica saturation, silica readily polymerizes into silanol [$Si(OH)_4$] groups which result in spiraling chains of silica polymers (Fig. 13a). Lower pH can be driven by either influx of fresh waters (Lovering and Patten, 1962; Knauth, 1979; Hesse, 1989; Knauth, 1994; Manning-Berg and Kah, 2017), or by the presence of organic acids within benthic microbial mats (Maliva and Siever, 1989; Konhauser, 2004; Lalonde et al., 2005; Shang et al., 2018). Once polymerization occurs, these elongate, silanol chains attach

tangentially to the growth surface, resulting in crystallographic c-axes that lie parallel to the surface, and perpendicular to the direction of fiber elongation (i.e., a length-fast orientation; Hauser, 1955; Iler, 1955; Alexander, 1967; Folk and Pittman, 1971; Iler, 1979).

Length-fast chalcedony, and its relationship to growth by addition of disordered polymer chains, is therefore a strong indicator of precipitation from a polymerized silica matrix, or siliceous gel (Iler, 1979; Sakka and Kamiya, 1982; Heaney, 1993; Lee, 2005). Crystal growth by the addition of such polymer chains also results in the increased incorporation of impurities (e.g., organic residues and trace elements) and bound non-

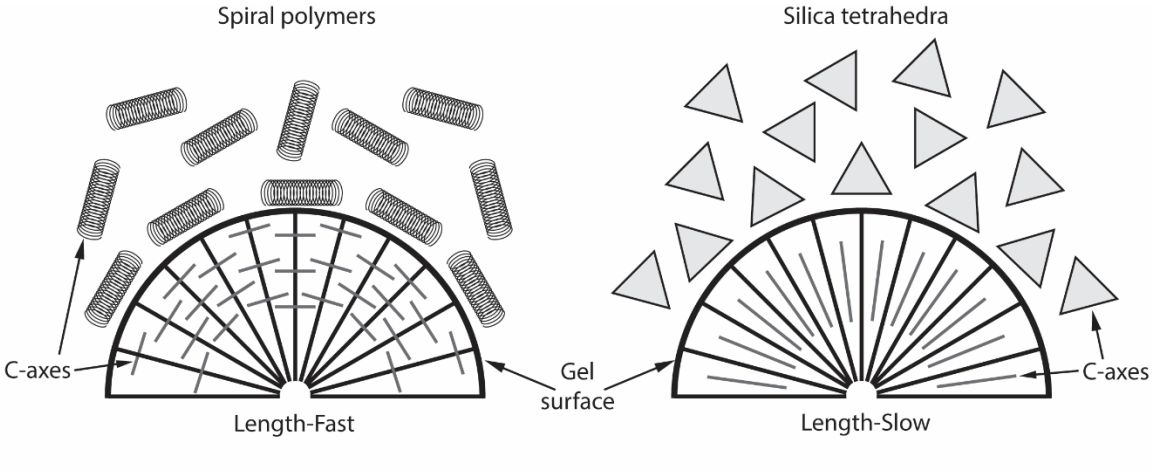

Fig. 13: Model for length-fast vs. length-slow fiber growth. Crystallite orientation (single tetrahedra versus spiral polymers) with respect to growth surface controls formation of length-slow vs. length-fast chalcedony crystals (modified from Folk and Pittman, 1971). Folk and Pittman (1971) used this model to explain the difference in crystallographic c-axis orientation of the two types of chalcedony. The illustration on the left represented polymerization under low pH conditions, whereby silica formed spiral chains that attached tangentially to the surface of a siliceous gel. Therefore, the c-axes lie parallel to the surface, and perpendicular to the direction of fiber elongation. The illustration on the right represents formation under high pH where silica is generally more ionized into single tetrahedra that subsequently attach to the growing surface individually, and result in fibers with c-axes parallel to the direction of fiber elongation.

structural water (Hauser, 1955; Folk and Pittman, 1971). As a result, length-fast chalcedony is often more hydrated than its length-slow counterpart, containing up to 1-4 wt% water (Frondel, 1982; Graetsch et al., 1985; Hesse, 1989; Heaney, 1993; Cady et al., 1996; Lee, 2005).

5.2 Silica Precipitation and Diagenesis

Experimental and observational data show that the silica precipitation generally initiates as nm-scale spherules of opal-A, which then converts to opal-CT and opal-C, and finally to quartz (Leo and Barghoorn, 1976; Williams et al., 1985; Hesse, 1989; Flörke et al., 1991; Heaney, 1993; Cady et al., 1996; Lynne and Campbell, 2004; Lee, 2005). These transitions, however, can follow a variety of different pathways.

Previous works have cited silica gels as the most likely precursor for crystallization of chalcedony in natural systems (Folk and Pittman, 1971; Williams et al., 1985; Hesse, 1989; Heaney, 1993), with the possible exception of deposition from silica springs, which contain outflow fluids that are highly supersaturated with respect to silica (Campbell et al., 2001; Lynne and Campbell, 2004). In either case, opal phases generally form rapidly in environments that are supersaturated with respect to silica, which results in crystallization with high-water content and greater disorder (Mizutani, 1966; Folk and Pittman, 1971; Stein and Kirkpartich, 1976; Williams et al. 1985; Cady and Wenk, 1989; Hesse, 1989; Heaney, 1993). Under these conditions, the primary opal-A phase can contain ≥10 wt% water within its structure (Graetsch et al. 1994; Graetsch & Ibel, 1997; Eckert et al., 2014).

Opal-CT is the most commonly observed intermediary opal phase, and is commonly observed as intermediate-sized (2-5 μm), bladed lepispheres (Flörke et al., 1976; Williams and Crerar, 1985; Cady et al., 1996; Hattori et al., 1996). Transmitted electron microscopy (TEM) observations suggest that the blades of opal-CT lepispheres actually consist of densely arrayed acicular fibers (Cady et al., 1996). The transition between opal-A and opal-CT most commonly results from dissolution-reprecipitation reactions as the saturation state of the parent solution decreases (Mizutani, 1966; Stein and Kirkpartich, 1976; Williams et al. 1985; Cady and Wenk, 1989; Maliva and Siever, 1989; Heaney, 1993). In some cases, however, TEM has revealed that both opal-CT and quartz may occasionally precipitate directly from solution as epitaxial overgrowths on microfibrous opal surfaces (Wenk et al. 1988; Cady et al., 1996).

The conversion of opal-A, through opal-CT, to quartz, however, involves substantial loss of bound water (Williams and Crerar, 1985; Flörke et al. 1991; Heaney, 1993; Cady et al., 1996). Water loss during the diagenetic transformation from opal-A to chalcedony is not conducive for preservation of primary fabrics (Oehler, 1976). By contrast, chalcedony spherules within Angmaat Formation chert mimetically preserve precursor fabrics.

An alternative mechanism of precipitation involves early precipitation as opal-CT (Maliva and Siever, 1989; Siever, 1992; Behl and Garrison, 1994; Cady et al., 1996). The crystallization of opal-CT ($\leq$8 wt% H_2O) to chalcedony (1-4 wt% H_2O) requires far less water loss, and may represent a more likely pathway for preservation of primary microbial mat elements. Under conditions that enhance polymerization of silica, behavior

of the silica gel becomes dependent upon the degree of cation cross-bridging between silanol groups (Iler, 1979; Heaney, 1993). In strongly polymerized gels, cross-linking results in reduced water content and a denser molecular framework of the gel. Under these conditions, direct precipitation of opal-CT can occur (Maliva and Siever, 1989; Heaney, 1993). The presence of specific cations may also enhance the direct precipitation of opal-CT. Magnesium, for instance, has been shown to both catalyze the conversion of opal-A to opal-CT and serve as nucleation sites for opal-CT (Kastner et al., 1977; Hesse, 1989). Under depositional conditions of the Angmaat Formation (i.e., hypersaline microbial flat with intermittent fresh-water influx; Manning-Berg and Kah, 2017), we propose conditions were favorable to formation of a potentially dense siliceous gel that could precipitate opal-CT without an opal-A precursor. The retention of spherulitic morphologies during conversion to chalcedony further suggests only minimal recrystallization by dissolution and reprecipitation, thus favoring mimetic preservation of the primary fabrics.

5.3 Variation in Spherulitic Fabrics

Predominance of spherulitic chalcedony in Angmaat Formation chert is readily recognized using gypsum plate, which highlights a rectilinear fabric resulting from packing of spherules. Spherulitic fabric is not particularly uncommon in chert and has been recognized in other Precambrian chert deposits (Maliva et al., 1989; Maliva et al., 2005). Similar rectilinear fabrics have also been recognized (Schubel and Simonson, 1990; Hattori et al., 1996; Camana et al., 2002). These fabrics have been most frequently described from evaporative alkaline lakes, such as that Lake Magadi, Kenya (Schubel and

Simonson, 1990), and in lakes associated with active volcanism (Hattori et al., 1996), that results in lacustrine waters extremely enriched in silica.

An early direct reference to a rectilinear fabric was presented by Schubel and Simonson (1990), who described the pervasive fabric within Magadiite chert as characterized by a "rectilinear" or "grid-work" pattern in crossed-polarized light with the gypsum plate inserted. The primary distinguishing characteristic of this fabric, which is optically discriminated from the surrounding equigranular microcrystalline quartz, is an apparent extinction in two directions at nearly perpendicular angles (Schubel and Simonson, 1990). Although Schubel and Simonson (1990) never directly recognized a spherulitic origin for the observed rectilinear fabric, they did note both the occurrence of this rectilinear fabric in thin sections cut in different orientations, which is consistent with a spherulitic origin. Estimates of crystal size (10-30 μm diameter; Schubel and Simonson, 1990) indicate spherules would have been much smaller than that observed in the Angmaat chert, which may have inhibited recognition of distinct spherules. An additional difference is in the mineralogical make-up of potential spherules. In Lake Magadi chert, Schubel and Simonson (1990) recognized the rectilinear fabric as having a length-slow orientation. They interpreted the length-slow nature of the chert to reflect recrystallization after the sodium silicate, Magadiite [$NaSi_7O_{13}(OH)_3 \bullet 4(H_2O)$].

Hattori et al. (1996) noted a similar rectilinear pattern in lacustrine silica deposits, but also recognized the presence of length-fast chalcedony spherules, ≤200 μm in diameter, that showed a brown coloration in plane-polarized light that had previously been attributed to incorporation of inclusions within opal-CT (cf. Behl and Garrison,

1994). Under SEM, Hattori et al. (1996) were able to show length-fast spherules being composed of individual <1μm opal-CT crystallites. Although Hattori et al. (1996) note the presence of both rectilinear fabric and chalcedony spherules, they do not draw a linkage between these two fabrics. Here, we suggest that a rectilinear fabric is a diagnostic characteristic of spherulitic chert. Care must be taken, however, to distinguish the spherulitic aspects of this fabric, including the presence of acicular chalcedony, and regions where sweeping extinction is visible.

For example, Camana et al. (2002) describe a rectilinear fabric in chert from ore-bearing siliceous crusts. This fabric, however, bears only superficial resemblance to the rectilinear fabric described here and elsewhere (Schubel and Simonson, 1990; Hattori et al., 1996). Rather, petrographic analyses performed by Camana et al., (2002) show well-formed, singly-terminated quartz crystals nucleating at angles on the faces of doubly-terminated quartz crystals producing an apparent grid or cross-like pattern.

Although this investigation of Angmaat chert does not provide substantial evidence for textures produced by the recrystallization of spherulitic chert at the present, we expect that even small amounts of recrystallization may result in difficulty in recognition of primary spherules. If diagenesis occurs under low water-rock ratios, however, individual acicular fibers with similar crystallographic orientations may simply recrystallize to single larger crystals. These crystals, however, would be expected to retain a clear length-fast (or length-slow) orientation, that could help diagnose the primary fabric.

5.4 Preservation of Primary Fabrics

The most remarkable aspect of spherulitic growth is the mimetic preservation of both microbial and mineral fabrics (cf. Kah and Knoll, 1996; Knoll et al., 2013). The size distributions of spherules are correlated with the density of organic staining, suggesting that organic matter may have played a fundamental role in the origin of spherulitic chert. Although we cannot distinguish the exact role, organic matter may have aided in nucleation either directly, by providing charged surfaces for nucleation, or passively, by enhancing the polymerization of silica and the formation of a densely networked silica gel. Unlike silica precipitation in thermal springs (Lynne and Campbell, 2004; Campbell et al., 2001), however, where silica nucleates as both opaline spheres within EPS sheaths and templates onto microbial surfaces (Konhauser, 2004; Lalonde et al., 2005), in Angmaat Formation chert fibrous radial spherules permeate primary fabrics and organic constituents (Fig. 8d). This suggests that nucleation originated within the matrix of the microbial mat, and was perhaps more strongly affected by the properties of the gel, and not simply the result of encrustation on the surfaces of organic matter.

It is also important to note that microbial fabrics within the Angmaat chert are largely represented by preserved sheaths of filamentous cyanobacteria (cf. Knoll et al., 2013). The preferential preservation of the polysaccharide sheaths of filaments, rather than the trichomes themselves, is common in preserved microbial communities (Horodyski, 1980; Horodyski, R.J. and Donaldson, J.A., 1980; Mendelson and Schopf, 1982; Allison and Awramik, 1989). We suggest that this common taphonomic state of microbial mats may, in fact, result from the silicification process. We suggest that the process of gel formation would stimulate the migration of motile microorganisms (i.e.,

primarily the filamentous microbes) away from the gelation front and toward the mat-water interface, potentially even driving expansion of a new mat on top of the silica gel. In this scenario, gel formation may not represent a single event, but a persistent process that operates synchronously with mat formation at the mat-water interface under conditions conducive to gel formation. The production of a siliceous gel could be stimulated by organic acids within the mat and associated EPS. Once motile organisms escaped, the silica gel could then permeate, or polymerize throughout, the empty microbial sheaths. In the absence of substantial evidence for sheath degradation, this scenario suggests that gel formation was complete on time-scales shorter than that of sheath degradation. We propose that, within this highly polymerized gel phase, precipitation of opal-CT crystallites would form. Syntaxial arrangement of these crystallites would permit individual complex chains of opal-CT—which would later diagenetically convert into length-fast chalcedony fibers—to permeate microbial elements without disruption of morphology.

Chalcedony spherules, however, also mimetically preserve aragonite fans. This suggests a siliceous gel also permeated spaces between aragonitic fibers, essentially encasing the fans within a gel matrix. In this model, gel formation must have occurred under environmental conditions (e.g., pH) insufficient for the rapid dissolution of aragonitic fibers. Because gels serve as buffers to pH change, it is likely that mimetic recrystallization proceeded by force of recrystallization (cf. Maliva and Siever, 1988), wherein the force exerted by a crystal growing from a solution or gel result in a decrease in solubility of material at the contact of this growing crystal. This results in the

incremental dissolution of the primary mineral phase, followed immediately by precipitation of the replacement mineral phase in its place. Such mechanism requires only minimal water-rock interaction and can result in fine-scale replacement. The presence of a gel phase that aids in the physical retention of insoluble organic materials would also support mimetic replacement.

CHAPTER SIX: CONCLUSIONS

Angmaat Formation chert is dominated by (≤200-10 μm) spherulitic length-fast chalcedony. The preserved fabrics are interpreted as crystallization, likely as opal-CT spherules, from a precursor silica gel phase, which could have occurred as a persistent penecontemporaneous silicifying front that migrated upwards with mat formation at the mat-water interface; as evidenced by the excellent preservation at several cm-depth within the mats. This silica gel phase provided a diffusion limiting matrix that supported spontaneous nucleation of spherules independently of microbial surfaces, and evidenced by limited Ostwald ripening. Spherulitic growth appears to be a common phenomenon in high-silica environments (e.g., volcanic; Hattori et al., 1996, and highly evaporative alkaline lakes; Schubel and Simons, 1990). Differences between length-fast and length-slow spherulitic chalcedony in these examples likely reflect differences in pH within the environment, where the circumneutral to low pH range has been observed to produce chalcedony with length-fast orientation; often associated with the dissolution of primary carbonate fabrics. As a result, not only does silicification have the potential for mimetic preservation of organic and mineral components, but also represents a process fundamentally different than templated mineralization of silica within thermal springs which may lend more insight into the conditions by which Proterozoic microfossiliferous chert forms.

REFERENCES

Alexandre, A., Meunier, J.D., Llorens, E., Hill, S.M., and Savin, S.M., 2004, Methodological improvements for investigating silcrete formation: petrography, FT-IR and oxygen isotope ratio of silcrete quartz cement, Lake Eyre Basin (Australia). Chemical Geology, v. 211, p. 261–274.

Alleon, J., Bernard, S., Le Guillou, C., Daval, D., Skouri-Panet, F., Pont, S., Delbes, L., and Robert, F., 2016, Early entombment within silica minimizes the molecular degradation of microorganisms during advanced diagenesis. Chemical Geology, v. 437, p. 98–108.

Allison, C.W. and Awramik, S.M., 1989, Organic-walled microfossils from earliest Cambrian or latest Proterozoic Tindir Group rocks, northwest Canada. Precambrian Research, v. 43(4), p.253-294.

Bartley, J.K., 1996, Actualistic taphonomy of cyanobacteria: implications for the Precambrian fossil record. Palaios, v. 11, p. 571–586.

Behl, R.J., and Garrison, R.E., 1994, August. The origin of chert in the Monterey Formation of California (USA). In Siliceous, phosphatic and glauconitic sediments of the Tertiary and Mesozoic: Proceedings of the 29th International Geological Congress, Part C, p.101-132.

Bernet, M., and Bassett, K., 2005, Provenance analysis by single-quartz-grain SEM-CL/optical microscopy. Journal of Sedimentary Research, v. 75, p. 492–500.

Bunaciu, A.A., Udriştioiu, E.G. and Aboul-Enein, H.Y., 2015, X-ray diffraction: instrumentation and applications. Critical Reviews in Analytical Chemistry, v. 45(4), p. 289-299.

Camana, G., Chateigner, D., Zucali, M. and Artioli, G., 2002, The grid-work texture of authigenic microcrystalline quartz in siliceous crust-type (SCT) mineralized horizons. American Mineralogist, v. 87(8-9), p. 1128-1138.

Campbell, K.A., Sannazzaro, K., Rodgers, K.A., Herdianita, N.R., and Browne, P.R.L., 2001, Sedimentary facies and mineralogy of the Late Pleistocene Umukuri silica sinter, Taupo Volcanic Zone, New Zealand: Journal of Sedimentary Research, v. 71, p. 727–746.

Clayton, C.J., Sieveking, G.D.G. and Hart, M.B., 1986, The chemical environment of flint formation in Upper Cretaceous chalks. In The scientific study of flint and chert, Cambridge: Cambridge University Press., v. 1, pp. 43-53.

DeMaster, D.J., 2003, The diagenesis of biogenic silica: chemical transformations occurring in the water column, seabed, and crust. Treatise on Geochemistry, v.7, p.407.

Den Brok, S.W.J. and Spiers, C.J., 1991, Experimental evidence for water weakening of quartzite by microcracking plus solution–precipitation creep. Journal of the Geological Society, v. 148(3), p.541-548.

Eckert, J., Gourdon, O., Jacob, D.E., Meral, C., Monteiro, P.J., Vogel, S.C., Wirth, R. and Wenk, H.R., 2015, Ordering of water in opals with different microstructures. European Journal of Mineralogy, v.27(2), p.203-213.

Flörke, O.W., Hollmann, R., Von Rad, U. and Rösch, H., 1976, Intergrowth and twinning in opal-CT lepispheres. Contributions to Mineralogy and Petrology, v.58(3), p.235-242.

Flörke, O.W., Graetsch, H., Röller, K., Martin, B. and Wirth, R., 1991, Nomenclature of micro-and non-crystalline silica minerals. Neues Jahrbuch für Mineralogie, Abhandlungen, v.163, p.19-42.

Folk, R.L. and Weaver, C.E., 1952, A study of the texture and composition of chert. American Journal of Science, v.250(7), p.498-510.

Foucher, F. and Westall, F., 2013, Raman imaging of metastable opal in carbonaceous microfossils of the 700– 800 Ma old Draken Formation. Astrobiology, v.13(1), p.57-67.

Frondel, C., 1978, Characters of quartz fibers. American mineralogist, v.63(1-2), p.17-27.

Frondel, C., 1982, Structural hydroxyl in chalcedony (type B quartz). American Mineralogist, v.67, p.1248-1257.

Ghasemi, A. and Zahediasl, S., 2012, Normality tests for statistical analysis: a guide for non-statisticians. International journal of endocrinology and metabolism, v.10(2), p.486.

Gibson, T.M., Shih, P.M., Cumming, V.M., Fischer, W.W., Crockford, P.W., Hodgskiss, M.S., Wörndle, S., Creaser, R.A., Rainbird, R.H., Skulski, T.M. and Halverson, G.P., 2017, Precise age of Bangiomorpha pubescens dates the origin of eukaryotic photosynthesis. Geology, v.46(2), p.135-138.

Götze, J., Plötze, M., Graupner, T., Hallbauer, D.K. and Bray, C.J., 2004, Trace element incorporation into quartz: a combined study by ICP-MS, electron spin resonance, cathodoluminescence, capillary ion analysis, and gas chromatography. Geochimica et Cosmochimica Acta, v.68(18), p.3741-3759.

Graetsch, H., Flörke, O.W. and Miehe, G., 1985, The nature of water in chalcedony and opal-C from Brazilian agate geodes. Physics and Chemistry of Minerals, v.12(5), p.300-306.

Graetsch, H., Flörke, O.W. and Miehe, G., 1987, Structural defects in microcrystalline silica. Physics and Chemistry of Minerals, v.14(3), p.249-257.

Graetsch, H., 1994, Structural characteristics of opaline and microcrystalline silica minerals. Reviews in Mineralogy and Geochemistry, v.29(1), p.209-232.

Graetsch, H. and Ibel, K., 1997, Small angle neutron scattering by opals. Physics and Chemistry of Minerals, v.24(2), p.102-108.

Hahn, K.E., Turner, E.C., Babechuk, M.G. and Kamber, B.S., 2015, Deep-water seep-related carbonate mounds in a Mesoproterozoic alkaline lake, Borden Basin (Nunavut, Canada). Precambrian Research, v.271, p.173-197.

Hattori, I., Umeda, M., Nakagawea, T. and Yamamoto, H., 1996, From chalcedonic chert to quartz chert; diagenesis of chert hosted in a Miocene volcanic-sedimentary succession, central Japan. Journal of Sedimentary Research, v.66(1), p.163-174.

Hauser, E.A., 1955, The Colloid Scince of Silica and Silicones. Silicic Science. New York: Van Nostrand, p.188.

Hesse, R., 1987, Selective and reversible carbonate—silica replacements in Lower Cretaceous carbonate-bearing turbidites of the Eastern Alps. Sedimentology, v.34(6), p.1055-1077.

Hesse, R., 1988, Diagenesis #13. Origin of chert: diagenesis of biogenic siliceous sediments. Geoscience Canada, v.15(3).

Hesse, R., 1989, Silica diagenesis: origin of inorganic and replacement cherts. Earth-Science Reviews, v.26(1), p.253-284.

Hippertt, J.F., 1994, Microstructures and c-axis fabrics indicative of quartz dissolution in sheared quartzites and phyllonites. Tectonophysics, v.229(3-4), p.141-163.

Hofman, H. J., and Jackson, G. D., 1991, Shelf-facies microfossils from the Uluksan Group (Proterozoic Bylot Supergroup), Baffin Island, Canada: Journal of Paleontology, v.65, p.361-381.

Hofmann, H.J. and Jackson, G.D., 1994, Shale-facies microfossils from the Proterozoic Bylot Supergroup, Baffin Island, Canada. Journal of Paleontology, v.68(S37), p.1-35.

Horodyski, R.J., 1980, Middle Proterozoic shale-facies microbiota from the lower Belt Supergroup, Little Belt Mountains, Montana. Journal of Paleontology, v. 5(4). p.649-663.

Horodyski, R.J. and Donaldson, J.A., 1980, Microfossils from the middle Proterozoic Dismal Lakes groups, arctic Canada. Precambrian Research, v.2, p.125-159.

Hüneke, H. and Henrich, R., 2011, Pelagic sedimentation in modern and ancient oceans. In Developments in sedimentology v.63, p. 215-351.

Ilieva, A., Mihailova, B., Tsintsov, Z. and Petrov, O., 2007. Structural state of microcrystalline opals: A Raman spectroscopic study. American Mineralogist, v.92(8-9), p.1325-1333.

Jackson, G.D. and Iannelli, T.R., 1981, Rift-related cyclic sedimentation in the Neohelikian Borden Basin, northern Baffin Island. Geological Survey of Canada, Paper, v.81(10), pp.269-302.

James, N.P., Narbonne, G.M. and Sherman, A.G., 1998, Molar-tooth carbonates: shallow subtidal facies of the Mid-to Late Proterozoic. Journal of Sedimentary Research, v.68(5), p.716-722.

Kah, L.C. and Knoll, A.H., 1996, Microbenthic distribution of Proterozoic tidal flats: environmental and taphonomic considerations. Geology, v.24(1), p.79-82.

Kah, L.C., 1997, Sedimentological, geochemical, and paleobiological interactions on a Mesoproterozoic carbonate platform: Society Cliffs Formation, northern Baffin Island, Arctic Canada, PhD thesis, Cambridge: Harvard University.

Kah, L.C., Sherman, A.G., Narbonne, G.M., Knoll, A.H. and Kaufman, A.J., 1999. δ13C stratigraphy of the Proterozoic Bylot Supergroup, Baffin Island, Canada: implications for regional lithostratigraphic correlations. Canadian Journal of Earth Sciences, v.36(3), p.313-332.

Kah, L.C., 2000, Depositional δ18O signatures in Proterozoic dolostones: constraints on seawater chemistry and early diagenesis.

Kah, L.C., Lyons, T.W. and Chesley, J.T., 2001, Geochemistry of a 1.2 Ga carbonate-evaporite succession, northern Baffin and Bylot Islands: implications for Mesoproterozoic marine evolution. Precambrian Research, v.111(1), p.203-234.

Kah, L.C., Bartley, J.K. and Teal, D.A., 2012, Chemostratigraphy of the Late Mesoproterozoic Atar Group, Taoudeni Basin, Mauritania: Muted isotopic variability, facies correlation, and global isotopic trends. Precambrian Research, 200, pp.82-103.

Kastner, M., Keene, J.B. and Gieskes, J.M., 1977, Diagenesis of siliceous oozes—I. Chemical controls on the rate of opal-A to opal-CT transformation—an experimental study. Geochimica et Cosmochimica Acta, v.41(8), p.1041-1059.

Kingma, K.J. and Hemley, R.J., 1994, Raman spectroscopic study of microcrystalline silica. American Mineralogist, v.79(3-4), p.269-273.

Knauth, L.P., 1979, A model for the origin of chert in limestone. Geology, v.7(6), p.274-277.

Knauth, L.P., 1994, Petrogenesis of chert. Reviews in Mineralogy and Geochemistry, v.29(1), p.233-258.

Knoll, A.H., Wörndle, S. and Kah, L.C., 2013, Covariance of microfossil assemblages and microbialite textures across an upper Mesoproterozoic carbonate platform. Palaios, v.28(7), p.453-470.

Konhauser, K.O., Jones, B., Phoenix, V.R., Ferris, G. and Renaut, R.W., 2004, The microbial role in hot spring silicification. AMBIO: A Journal of the Human Environment, v.33(8), p.552-558.

Lalonde, S.V., Konhauser, K.O., REYSENBACH, A.L. and Ferris, F.G., 2005, The experimental silicification of Aquificales and their role in hot spring sinter formation. Geobiology, v.3(1), p.41-52.

Langer, K. and Flörke, O.W., 1974, Near infrared absorption spectra (4000–9000 cm− 1) of opals and the role of “water” in these SiO 2· nH 2 O minerals. Fortschritte der Mineralogie, v.52(1), p.17-51.

LeCheminant, A.N. and Heaman, L.M., 1989, Mackenzie igneous events, Canada: Middle Proterozoic hotspot magmatism associated with ocean opening. Earth and Planetary Science Letters, v.96(1-2), p.38-48.

Lee, D.R., 2005, Characterisation and the diagenetic transformation of non-and micro-crystalline silica minerals. Department of Earth and Ocean Sciences, University of Liverpool, v.1, p.20.

Leo, R.F. and Barghoorn, E.S., 1976, Silicification of wood. Botanical Museum Leaflets, Harvard University, v.25(1), p.1-47.

Lovering, T.G. and Patten, L.E., 1962, The effect of CO2 at low temperature and pressure on solutions supersaturated with silica in the presence of limestone and dolomite. Geochimica et Cosmochimica Acta, v.26(7), p.787-796.

Lynne, B.Y. and Campbell, K.A., 2004, Morphologic and mineralogic transitions from opal-A to opal-CT in low-temperature siliceous sinter diagenesis, Taupo Volcanic Zone, New Zealand. Journal of Sedimentary Research, v.74(4), p.561-579.

MacDonald, J., Freer, A. and Cusack, M., 2009, Alignment of crystallographic c-axis throughout the four distinct microstructural layers of the oyster Crassostrea gigas. Crystal Growth and Design, v.10(3), p.1243-1246.

Maitland, T. and Sitzman, S., 2007, Electron backscatter diffraction (EBSD) technique and materials characterization examples, Berlin: Springer, v.14, p. 522.

Maliva, R.G., 1985, An early diagenetic model for the origin of geodes in the Ramp Creek Formation and Harrodsburg Limestone (Mississippian), southern Indiana. In Geological Society of America Abstracts with Programs, v.l(17), p. 300.

Maliva, R.G. and Siever, R., 1988, Diagenetic replacement controlled by force of crystallization. Geology, v.16(8), p.688-691.

Maliva, R.G., Knoll, A.H. and Siever, R., 1989, Secular change in chert distribution: a reflection of evolving biological participation in the silica cycle. Palaios, v.4(6), p.519-532.

Maliva, R.G. and Siever, R., 1989, Nodular chert formation in carbonate rocks. The Journal of Geology, v.97(4), p.421-433.

Maliva, R.G., Knoll, A.H. and Simonson, B.M., 2005, Secular change in the Precambrian silica cycle: insights from chert petrology. Geological Society of America Bulletin, v.7-8, p.835-845.

Manning-Berg, A.R. and Kah, L.C., 2017, Proterozoic microbial mats and their constraints on environments of silicification. Geobiology, v.15(4), p.469-483.

Mateen, T., Rehman, H.U. and Yamamoto, H., 2013, EBSD study of Quartz c-axis orientations in the silicified host rocks of the Kasuga gold deposit, Southwest Japan. Journal of Mineralogical and Petrological Sciences, v.108(5), p.278-287.

Mendelson, C.V. and Schopf, J.W., 1982, Proterozoic microfossils from the Sukhaya Tunguska, Shorikha, and Yudoma Formations of the Siberian platform, USSR. Journal of Paleontology, v.55(1), p.42-83.

Milliken, K.L., 1979, The silicified evaporite syndrome--two aspects of silicification history of former evaporite nodules from southern Kentucky and northern Tennessee. Journal of Sedimentary Research, v.49(1), p.245-256.

Milliken, K.L. and Laubach, S.E., 2000, Brittle deformation in sandstone diagenesis as revealed by scanned cathodoluminescence imaging with application to characterization of fractured reservoirs. In Cathodoluminescence in geosciences, p. 225-243.

Murata, K.J. and Nakata, J.K., 1974, Cristobalitic stage in the diagenesis of diatomaceous shale. Science, v.184(4136), p.567-568.

Oehler, J.H. and Schopf, J.W., 1971, Artificial microfossils: experimental studies of permineralization of blue-green algae in silica. Science, v.174(4015), p.1229-1231.

Oehler, J.H., 1975, Origin and distribution of silica lepispheres in porcelanite from the Monterey Formation of California. Journal of Sedimentary Research, v.45(1), p.252-257.

Oehler, J.H., 1976, Experimental studies in Precambrian paleontology: structural and chemical changes in blue-green algae during simulated fossilization in synthetic chert. Geological Society of America Bulletin, v.87(1), p.117-129.

Oehler, J.H. and Logan, R.G., 1977, Microfossils, cherts, and associated mineralization in the Proterozoic McArthur (HYC) lead-zinc-silver deposit. Economic Geology, v.72(8), p.1393-1409.

Olcott Marshall, A. and Marshall, C.P., 2015, Vibrational spectroscopy of fossils. Palaeontology, v.58(2), p.201-211.

Pannirselvam, M., Garg, A., Tardio, J., Antolasic, F., Grocott, S. and Bhargava, S., 2009, Mineral characterization using micro x-ray diffraction (micro XRD), a state-of-the-art non-destructive technique. Engineering Our Future: Are We up to the Challenge?: 27-30 September 2009, Burswood Entertainment Complex, p.11-19.

Pehrsson, S.J. and Buchan, K.L., 1999, Borden dykes of Baffin Island, Northwest Territories: a Franklin U-Pb baddeleyite age and a paleomagnetic reinterpretation. Canadian Journal of Earth Sciences, v.36(1), p.65-73.

Pérez-Huerta, A., Dauphin, Y., Cuif, J.P. and Cusack, M., 2011, High resolution electron backscatter diffraction (EBSD) data from calcite biominerals in recent gastropod shells. Micron, v.42(3), p.246-251.

Post, J.E., Bish, D.L. and Heaney, P.J., 2007, Synchrotron powder X-ray diffraction study of the structure and dehydration behavior of sepiolite. American Mineralogist, v.92(1), p.91-97.

Schmitt, J. and Flemming, H.C., 1998, FTIR-spectroscopy in microbial and material analysis. International Biodeterioration and Biodegradation, v.41(1), p.1-11.

Schopf, J.W., 1993, Microfossils of the Early Archean Apex chert: new evidence of the antiquity of life. Science, v.260(5108), p.640-646.

Schopf, J.W., Tewari, V.C. and Kudryavtsev, A.B., 2008, Discovery of a new Chert-Permineralized Microbiota in the Proterozoic Buxa Formation of the Ranjit window, Sikkim, northeast India, and its astrobiological implications. Astrobiology, v.8(4), p.735-746.

Schubel, K.A. and Simonson, B.M., 1990, Petrography and diagenesis of cherts from Lake Magadi, Kenya. Journal of Sedimentary Research, v.60(5), p.761-776.

Shang, X., Moczydłowska, M., Liu, P. and Liu, L., 2018, Organic composition and diagenetic mineralization of microfossils in the Ediacaran Doushantuo chert nodule by Raman and petrographic analyses. Precambrian Research, v.314, p.145-159.

Sherman, A.G., Narbonne, G.M. and James, N.P., 2001, Anatomy of a cyclically packaged Mesoproterozoic carbonate ramp in northern Canada. Sedimentary Geology, v.139(3), p.171-203.

Siever, R., 1962, A squeezer for extracting interstitial water from modern sediments. Journal of Sedimentary Research, v.32(2), p.329-331.

Siever, R., 1992, The silica cycle in the Precambrian. Geochimica et Cosmochimica Acta, v.56(8), p.3265-3272.

Simonson, B.M., 1985, Sedimentology of cherts in the Early Proterozoic Wishart Formation, Quebec-Newfoundland, Canada. Sedimentology, v.32(1), p.23-40.

Southgate, P.N., 1986, Depositional environment and mechanism of preservation of microfossils, upper Proterozoic Bitter Springs Formation, Australia. Geology, v.14(8), p.683-686.

Stein, C.L., 1982, Silica recrystallization in petrified wood. Journal of Sedimentary Research, v.52(4), p.1277-1282.

Turner, E.C., 2009, Mesoproterozoic carbonate systems in the Borden Basin, Nunavut. Canadian Journal of Earth Sciences, v.46(12), p.915-938.

Turner, E.C. and Kamber, B.S., 2012, Arctic Bay Formation, Borden Basin, Nunavut (Canada): Basin evolution, black shale, and dissolved metal systematics in the Mesoproterozoic ocean. Precambrian Research, v.208, p.1-18.

Tyler, S.A. and Barghoorn, E.S., 1954, Occurrence of structurally preserved plants in pre-Cambrian rocks of the Canadian Shield. Science, v.119(3096), p.606-608.

Walker, T.R., 1962, Reversible nature of chert-carbonate replacement in sedimentary rocks. Geological Society of America Bulletin, v.73(2), p.237-242.

Weil, J.A., 1984, A review of electron spin spectroscopy and its application to the study of paramagnetic defects in crystalline quartz. Physics and Chemistry of Minerals, v.10(4), p.149-165.

Weil, J.A., 1993, A review of the EPR spectroscopy of the point defects in α-quartz: the decade 1982–1992. In The Physics and Chemistry of SiO2 and the Si-SiO2 Interface 2, p. 131-144.

Williams, L.A., Parks, G.A. and Crerar, D.A., 1985, Silica diagenesis; I, Solubility controls. Journal of Sedimentary Research, v.55(3), p.301-311.

Williams, L.A. and Crerar, D.A., 1985, Silica diagenesis, II. General mechanisms. Journal of Sedimentary Research, v.55(3), p.301-311.

Wilson, R.C.L., 1966, Silica diagenesis in Upper Jurassic limestones of southern England. Journal of Sedimentary Research, v.36(4), p.1036-1049.

APPENDIX

	Name	Alternative names	Description	Citations
Non-crystalline (Sub-crystalline)	Opal-A	N/A	Amorphous opals; only present when system is very supersaturated with resepect to silica. Presents very weak x-ray diffraction pattern, indicating that crystallographic order is very local. Readily converted into more ordered phases with dewatering under low diagenesis.	Heaney, 1993; Foucher and Westal, 2013
	Opal-CT	lussatine	Microcrystalline opals made of intergrown cristobalite and tridymite	Graetsch, 1994; Flörke et al., 1991; Flörke et al., 1973
	Opal-C	lussatite	Microcrystalline opals made of cristobalite	Graetsch, 1994; Flörke et al., 1991; Flörke et al., 1973
Granular	Microcrystalline Quartz	microquartz	Tiny crystals of quartz (generally < 5 to 20 microns), display an equigranular texture with pin-point extinction.	Hesse, 1989; Folk and Pittman, 1971
	Megaquartz	N/A	Size range from 20 to >2000 microns). Similar fabric to drusy calcite mosaics. Commonly increasing in crystal size from edge of voids to centre.	Hesse, 1989
	Moganite	Lutecite, Lutecine	Cryptocrystalline, often intergrown with quartz in chalcedony. Moganite growth more prevalent in evaporite-type cherts. Appears to be converted to chalcedony over time.	Götze et al., 1998; Heaney and Post, 1992; Flörke et al., 1976
Fibrous	Length-Fast Chalcedony	Chalcedony sensu stricto, Luticite	Mineral crystallites grow perpendincular to mineral elongation. Frequently seen to grow in a radiating pattern from a single point (typically as void-filling).	Hesse, 1989
	Length-Slow Chalcedony	Quartzine	Elongation of the fibers is parallel with the crystallographic C-axis. This fabric occurs in chert nodules, often replacing former evaporites.	Hesse, 1989; Michel-Levy and Munier-Chalmas, 1892
	Microflamboyant	Flamboyant lutecite	An intermediate phase between equant and fibrous quartz types. Displays undulose extinction caused by composite, fanning crystals; individual crystal boundaries not clearly recognizable.	Hesse, 1989; Milliken, 1979; Folk and Pittman, 1971
	Zebraic Chalcedony		Displays a banded extinction pattern under crossed polarized light, as the stage is rotated through extinction.	Hesse, 1989; McBride and Folk, 1977; Frondel, 1978

Compiled "Red"				
Label	**Area**	**Angle**	**Length (mm)**	**Length (µm)**
JID.004.20xGY(9?5)BLUE.tif	1.56E-05	-98.397	0.057	57
JID.004.20xGY(9?5)BLUE.tif	1.33E-05	-99.772	0.049	49
JID.004.20xGY(9?5)BLUE.tif	1.78E-05	-99.424	0.066	66
JID.004.20xGY(9?5)BLUE.tif	1.79E-05	-86.482	0.066	66
JID.004.20xGY(9?5)BLUE.tif	1.40E-05	-101.368	0.052	52
JID.004.20xGY(9?5)BLUE.tif	1.08E-05	-99.398	0.04	40
JID.004.20xGY(9?5)BLUE.tif	1.07E-05	-95.123	0.039	39
JID.004.20xGY(9?5)BLUE.tif	1.36E-05	-105.228	0.05	50
JID.004.20xGY(9?5)BLUE.tif	1.08E-05	-121.557	0.04	40
JID.004.20xGY(9?5)BLUE.tif	1.02E-05	-90	0.037	37
JID.004.20xGY(9?5)BLUE.tif	9.66E-06	-99.605	0.035	35
JID.004.20xGY(9?5)BLUE.tif	1.18E-05	-73.131	0.044	44
JID.004.20xGY(9?5)4.jpeg	1.90E-05	-103.717	0.07	70
JID.004.20xGY(9?5)4.jpeg	1.29E-05	-94.844	0.048	48
JID.004.20xGY(9?5)4.jpeg	1.71E-05	-99.1	0.063	63
JID.004.20xGY(9?5)4.jpeg	1.17E-05	-100.049	0.043	43
JID.004.20xGY(9?5)4.jpeg	1.02E-05	-83.434	0.038	38
JID.004.20xGY(9?5)4.jpeg	1.16E-05	-106.144	0.042	42
JID.004.20xGY(9?5)4.jpeg	1.32E-05	-95.742	0.049	49
JID.004.20xGY(9?5)4.jpeg	5.96E-06	-98.531	0.022	22
JID.004.20xGY(9?5)4.jpeg	8.94E-06	-98.531	0.033	33
JID.004.20xGY(9?5)4.jpeg	4.12E-05	-102.045	0.152	152
JID.004.10xGY(9?5)3.jpeg	4.47E-05	-91.109	0.083	83
JID.004.10xGY(9?5)3.jpeg	2.61E-05	-88.091	0.048	48
JID.004.10xGY(9?5)3.jpeg	3.35E-05	-98.896	0.062	62
JID.004.10xGY(9?5)3.jpeg	4.24E-05	-99.398	0.079	79
JID.004.10xGY(9?5)3.jpeg	5.01E-05	-96.267	0.093	93
JID.004.10xGY(9?5)3.jpeg	3.01E-05	-102.171	0.056	56
JID.004.10xGY(9?5)3.jpeg	4.53E-05	80.779	0.084	84
JID.004.10xGY(9?5)3.jpeg	4.15E-05	-98.746	0.077	77
JID.004.10xGY(9?5)3.jpeg	2.72E-05	-99.26	0.05	50
JID.004.10xGY(9?5)3.jpeg	4.12E-05	-85.972	0.076	76
JID.004.10xGY(9?5)3.jpeg	7.88E-05	-96.502	0.147	147
JID.004.10xGY(9?5)3.jpeg	3.32E-05	-94.514	0.061	61
JID.004.10xGY(9?5)3.jpeg	3.90E-05	-110.056	0.072	72
JID.004.20xGY(9?5)6.jpeg	1.13E-05	-93.715	0.042	42
JID.004.20xGY(9?5)6.jpeg	8.94E-06	-81.539	0.033	33
JID.004.20xGY(9?5)6.jpeg	9.37E-06	-105.452	0.035	35

JID.004.20xGY(9?5)6.jpeg	9.95E-06	-92.526	0.037	37
JID.004.20xGY(9?5)6.jpeg	1.90E-05	-94.18	0.07	70
JID.004.20xGY(9?5)6.jpeg	7.48E-06	-95.042	0.028	28
JID.004.20xGY(9?5)6.jpeg	8.14E-06	-109.411	0.03	30
JID.004.20xGY(9?5)6.jpeg	6.39E-06	-96.633	0.023	23
JID.004.40xGY(9?5)5.jpeg	1.00E-05	-106.39	0.075	75
JID.004.40xGY(9?5)5.jpeg	9.79E-06	-98.628	0.074	74
JID.004.40xGY(9?5)5.jpeg	9.10E-06	-100.394	0.068	68
JID.004.40xGY(9?5)5.jpeg	6.79E-06	-100.812	0.051	51
JID.004.40xGY(9?5)5.jpeg	1.26E-05	-101.263	0.095	95
JID.004.40xGY(9?5)5.jpeg	6.09E-06	-101.897	0.046	46
JID.005.10xGY2.jpeg	3.09E-05	-101.725	0.057	57
JID.005.10xGY2.jpeg	6.27E-05	-95.816	0.116	116
JID.005.10xGY2.jpeg	3.55E-05	-101.674	0.066	66
JID.005.10xGY2.jpeg	2.75E-05	-101.547	0.051	51
JID.005.10xGY2.jpeg	2.72E-05	-99.26	0.05	50
JID.005.10xGY2.jpeg	4.38E-05	-95.673	0.081	81
JID.005.10xGY2.jpeg	2.52E-05	-96.633	0.047	47
JID.005.10xGY2.jpeg	2.86E-05	-91.736	0.053	53
JID.005.10xGY2.jpeg	3.21E-05	-102.529	0.059	59
JID.005.10xGY1.jpeg	2.73E-05	-99.762	0.05	50
JID.005.10xGY1.jpeg	2.44E-05	-98.902	0.045	45
JID.005.10xGY1.jpeg	2.84E-05	-100.62	0.052	52
JID.005.10xGY1.jpeg	3.33E-05	-97.921	0.062	62
JID.005.10xGY1.jpeg	2.59E-05	-104.191	0.048	48
JID.005.10xGY1.jpeg	3.16E-05	-96.864	0.058	58
JID.005.10xGY1.jpeg	1.75E-05	-101.689	0.032	32
JID.005.10xGY1.jpeg	2.73E-05	-99.762	0.05	50
JID.005.10xGY1.jpeg	1.90E-05	-95.274	0.035	35
JID.005.10xGY1.jpeg	2.16E-05	-92.322	0.04	40
JID.005.10xGY1.jpeg	2.70E-05	-95.587	0.05	50
JID.005.10xGY1.jpeg	3.45E-05	-97.787	0.064	64
JID.005.10xGY1.jpeg	2.56E-05	-100.539	0.047	47
JID.005.10xGY1.jpeg	2.36E-05	-99.23	0.044	44
JID.005.10xGY1.jpeg	2.18E-05	-99.964	0.04	40
JID.005.10xGY1.jpeg	1.98E-05	-92.526	0.036	36
JID.006.20xGY3.jpeg	9.01E-06	-100.305	0.033	33
JID.006.20xGY3.jpeg	1.27E-05	-94.297	0.047	47
JID.006.20xGY3.jpeg	7.27E-06	-91.736	0.027	27
JID.006.20xGY3.jpeg	6.47E-06	-99.894	0.024	24
JID.006.20xGY3.jpeg	9.52E-06	-95.711	0.035	35

JID.006.20xGY3.jpeg	1.16E-05	-96.54	0.043	43
JID.006.20xGY3.jpeg	5.96E-06	-94.289	0.022	22
JID.006.20xGY3.jpeg	9.15E-06	-96.897	0.034	34
JID.006.20xGY3.jpeg	8.65E-06	-95.807	0.032	32
JID.006.20xGY3.jpeg	4.80E-06	-90	0.017	17
JID.006.20xGY3.jpeg	7.56E-06	-96.71	0.028	28
JID.006.20xGY3.jpeg	6.83E-06	-93.691	0.025	25
JID.006.20xGY3.jpeg	8.28E-06	-99.713	0.03	30
JID.005.20xGY2.jpeg	1.88E-05	-101.179	0.07	70
JID.005.20xGY2.jpeg	2.06E-05	-92.445	0.076	76
JID.005.20xGY2.jpeg	1.50E-05	-98.641	0.056	56
JID.005.20xGY2.jpeg	1.39E-05	-96.34	0.051	51
JID.005.20xGY2.jpeg	8.72E-06	-99.147	0.032	32
JID.005.20xGY2.jpeg	9.08E-06	-86.743	0.033	33
JID.005.20xGY2.jpeg	1.42E-05	-98.881	0.052	52
JID.005.20xGY1.jpeg	1.58E-05	-99.028	0.058	58
JID.005.20xGY1.jpeg	1.43E-05	-102.054	0.053	53
JID.005.20xGY1.jpeg	1.85E-05	-108.577	0.069	69
JID.005.20xGY1.jpeg	1.64E-05	-98.669	0.061	61
JID.005.20xGY1.jpeg	9.74E-06	-94.3	0.036	36
JID.005.20xGY1.jpeg	1.42E-05	-110.487	0.052	52
JID.005.20xGY1.jpeg	1.33E-05	-99.772	0.049	49
JID.005.20xGY1.jpeg	1.29E-05	-102.072	0.048	48
JID.005.20xGY2.jpeg	2.12E-05	-95.123	0.079	79
JID.005.20xGY2.jpeg	1.90E-05	-102.433	0.07	70
JID.005.20xGY2.jpeg	1.50E-05	-96.987	0.055	55
JID.005.20xGY2.jpeg	1.30E-05	-97.765	0.048	48
JID.005.20xGY2.jpeg	1.16E-05	-94.371	0.043	43
JID.005.20xGY2.jpeg	8.21E-06	-96.17	0.03	30
JID.005.20xGY2.jpeg	1.02E-05	-97.784	0.038	38
JID.005.20xGY2.jpeg	1.16E-05	-96.499	0.043	43
JID.006.20xGY1.jpeg	7.77E-06	-96.459	0.029	29
JID.006.20xGY1.jpeg	5.59E-06	-101.459	0.02	20
JID.006.20xGY1.jpeg	4.36E-06	-95.807	0.016	16
JID.006.20xGY1.jpeg	6.97E-06	-101.07	0.025	25
JID.006.20xGY1.jpeg	6.54E-06	-104.191	0.024	24
JID.006.20xGY1.jpeg	8.06E-06	-99.462	0.03	30
JID.006.20xGY1.jpeg	5.67E-06	-92.231	0.021	21
JID.006.20xGY1.jpeg	7.56E-06	-111.077	0.028	28
JID.006.20xGY1.jpeg	7.05E-06	-93.576	0.026	26
JID.006.20xGY1.jpeg	7.56E-06	-98.286	0.028	28

JID.006.20xGY1.jpeg	6.83E-06	-93.731	0.025	25
JID.006.20xGY2.jpeg	8.43E-06	-97.496	0.031	31
JID.006.20xGY2.jpeg	7.85E-06	-101.834	0.029	29
JID.006.20xGY2.jpeg	7.99E-06	-94.764	0.029	29
JID.006.20xGY2.jpeg	8.86E-06	-102.888	0.033	33
JID.006.20xGY2.jpeg	7.05E-06	-93.614	0.026	26
JID.006.20xGY2.jpeg	5.59E-06	-104.4	0.021	21
JID.006.20xGY2.jpeg	5.74E-06	-94.456	0.021	21
JID.006.20xGY2.jpeg	7.34E-06	-96.911	0.027	27
JID.006.20xGY2.jpeg	6.83E-06	-91.848	0.025	25
JID.006.20xGY2.jpeg	8.86E-06	-92.862	0.033	33
JID.006.20xGY2.jpeg	9.59E-06	-97.883	0.035	35
JID.006.20xGY2.jpeg	7.85E-06	-100.257	0.029	29
JID.006.20xGY2.jpeg	1.07E-05	-102.315	0.039	39
JID.006.20xGY2.jpeg	6.39E-06	-97.853	0.024	24
JID.006.20xGY2.jpeg	7.99E-06	-97.907	0.029	29
JID.006.20xGY2.jpeg	7.05E-06	-105.046	0.026	26
JID.006.20xGY2.jpeg	7.77E-06	-98.664	0.029	29
JID.006.20xGY2.jpeg	8.50E-06	-99.382	0.031	31
JID.006.20xGY2.jpeg	1.37E-05	-97.696	0.05	50
JID.006.20xGY2.jpeg	1.20E-05	-100.899	0.044	44
JID.006.20xGY2_IJ2_BLUE.tif	8.50E-06	-99.462	0.031	31
JID.006.20xGY2_IJ2_BLUE.tif	7.48E-06	-91.685	0.028	28
JID.006.20xGY2_IJ2_BLUE.tif	9.08E-06	-95.528	0.033	33
JID.006.20xGY2_IJ2_BLUE.tif	7.70E-06	-91.621	0.028	28
JID.006.20xGY2_IJ2_BLUE.tif	6.39E-06	-95.906	0.023	23
JID.006.20xGY2_IJ2_BLUE.tif	7.12E-06	-97.125	0.026	26
JID.006.20xGY2_IJ2_BLUE.tif	5.23E-06	-94.83	0.019	19
JID.006.20xGY2_IJ2_BLUE.tif	8.43E-06	-97.431	0.031	31
JID.006.20xGY2_IJ2_BLUE.tif	7.34E-06	-98.616	0.027	27
JID.006.20xGY2_IJ2_BLUE.tif	8.94E-06	-98.997	0.033	33
JID.006.20xGY2_IJ2_BLUE.tif	6.90E-06	-97.958	0.025	25
JID.006.20xGY2_IJ2_BLUE.tif	7.99E-06	-98.427	0.029	29
JID.006.20xGY2_IJ2_BLUE.tif	8.72E-06	-98.746	0.032	32
JID.006.20xGY2_IJ2_BLUE.tif	6.97E-06	-102.724	0.026	26
JID.006.20xGY2_IJ2_BLUE.tif	7.19E-06	-100.62	0.026	26
JID.006.20xGY2_IJ2_BLUE.tif	6.39E-06	-106.763	0.023	23
JID.006.20xGY2_IJ2_BLUE.tif	7.99E-06	-96.34	0.029	29
JID.006.20xGY2_IJ2_BLUE.tif	7.92E-06	-91.591	0.029	29
JID.006.20xGY2_IJ2_BLUE.tif	1.07E-05	-97.076	0.039	39
JID.006.20xGY2_IJ2_BLUE.tif	7.12E-06	-97.712	0.026	26

JID.006.20xGY2_IJ2_BLUE.tif	7.41E-06	-102.095	0.027	27
JID.006.20xGY2_IJ2_BLUE.tif	1.13E-05	-100.072	0.042	42
JID.006.20xGY2_IJ2_BLUE.tif	1.32E-05	-96.654	0.049	49
JID.006.20xGY2_IJ2_BLUE.tif	1.21E-05	-97.297	0.045	45
JID.006.20xGY2_IJ2_BLUE.tif	7.92E-06	-93.18	0.029	29
JID.006.20xGY2_IJ2_BLUE.tif	7.12E-06	-97.125	0.026	26
JID.006.40xGY2.jpeg	2.93E-06	-102.943	0.022	22
JID.006.40xGY2.jpeg	3.72E-06	-92.454	0.028	28
JID.006.40xGY2.jpeg	3.86E-06	-96.572	0.029	29
JID.006.40xGY2.jpeg	2.65E-06	-103.109	0.02	20
JID.006.40xGY2.jpeg	3.44E-06	-103.679	0.026	26
JID.006.40xGY2.jpeg	3.76E-06	-97.595	0.028	28
JID.006.40xGY2.jpeg	3.58E-06	-96.809	0.027	27
JID.006.40xGY2.jpeg	3.02E-06	-91.011	0.023	23
JID.011.20xGY(9?5).jpeg	8.65E-06	-95.807	0.032	32
JID.011.20xGY(9?5).jpeg	1.41E-05	-95.681	0.052	52
JID.011.20xGY(9?5).jpeg	1.02E-05	-97.379	0.038	38
JID.011.20xGY(9?5).jpeg	8.14E-06	-102.918	0.03	30
JID.011.20xGY(9?5).jpeg	8.06E-06	-99.978	0.03	30
JID.011.20xGY(9?5).jpeg	9.15E-06	-98.781	0.034	34
JID.011.20xGY(9?5).jpeg	1.24E-05	-103.707	0.045	45
JID.011.20xGY(9?5).jpeg	1.94E-05	-90.646	0.072	72
JID.006.20xGY3.jpeg	1.24E-05	-100.516	0.046	46
JID.006.20xGY3.jpeg	1.13E-05	-99.34	0.041	41
JID.006.20xGY3.jpeg	9.81E-06	-98.13	0.036	36
JID.006.20xGY3.jpeg	7.70E-06	-88.363	0.028	28
JID.006.20xGY3.jpeg	6.90E-06	-97.958	0.025	25
JID.006.20xGY3.jpeg	7.85E-06	-99.728	0.029	29
JID.006.20xGY3.jpeg	7.12E-06	-97.125	0.026	26
JID.006.20xGY3.jpeg	8.94E-06	-98.461	0.033	33
JID.006.20xGY3.jpeg	8.86E-06	-94.289	0.033	33
JID.006.20xGY3.jpeg	7.12E-06	-97.125	0.026	26
JID.006.20xGY3.jpeg	6.83E-06	-93.691	0.025	25
JID.006.20xGY3.jpeg	7.48E-06	-90	0.028	28
JID.006.20xGY3.jpeg	5.09E-06	-97.539	0.019	19
JID.011.20xGY(9?7).jpeg	1.36E-05	-95.528	0.05	50
JID.011.20xGY(9?7).jpeg	1.98E-05	-88.736	0.073	73
JID.011.20xGY(9?7).jpeg	9.30E-06	-90	0.034	34
JID.011.20xGY(9?7).jpeg	8.21E-06	-96.17	0.03	30
JID.011.20xGY(9?7).jpeg	1.48E-05	-97.09	0.055	55
JID.011.20xGY(9?7).jpeg	1.27E-05	-94.927	0.047	47

JID.011.20xGY(9?7).jpeg	1.34E-05	-94.997	0.049	49
JID.011.20xGY(9?7).jpeg	1.23E-05	-102.714	0.045	45

Compiled "Blue"				
Label	Area	Angle	Length (mm)	Length (µm)
JID.004.20xGY(9?5).jpeg	1.34E-05	-5.648	0.049	49
JID.004.20xGY(9?5).jpeg	1.59E-05	-5.004	0.059	59
JID.004.20xGY(9?5).jpeg	1.63E-05	-9.59	0.06	60
JID.004.20xGY(9?5).jpeg	1.34E-05	-16.759	0.05	50
JID.004.20xGY(9?5).jpeg	1.50E-05	-18.435	0.055	55
JID.004.20xGY(9?5).jpeg	1.29E-05	-18.538	0.047	47
JID.004.20xGY(9?5).jpeg	9.44E-06	-11.222	0.035	35
JID.004.20xGY(9?5).jpeg	1.05E-05	-6.384	0.039	39
JID.004.20xGY(9?5).jpeg	1.11E-05	-26.565	0.041	41
JID.004.20xGY(9?5).jpeg	8.14E-06	0	0.03	30
JID.004.20xGY(9?5).jpeg	9.95E-06	-2.946	0.037	37
JID.004.20xGY(9?5).jpeg	6.83E-06	0	0.025	25
JID.004.20xGY(9?5)4.jpeg	1.91E-05	-8.099	0.071	71
JID.004.20xGY(9?5)4.jpeg	1.57E-05	-11.834	0.058	58
JID.004.20xGY(9?5)4.jpeg	1.69E-05	2.222	0.063	63
JID.004.20xGY(9?5)4.jpeg	1.29E-05	-12.072	0.048	48
JID.004.20xGY(9?5)4.jpeg	1.05E-05	-12.572	0.038	38
JID.004.20xGY(9?5)4.jpeg	9.30E-06	-4.054	0.034	34
JID.004.20xGY(9?5)4.jpeg	8.14E-06	3.608	0.03	30
JID.004.20xGY(9?5)4.jpeg	5.81E-06	-13.861	0.021	21
JID.004.20xGY(9?5)4.jpeg	7.99E-06	-6.801	0.029	29
JID.004.20xGY(9?5)4.jpeg	1.54E-05	-10.886	0.057	57
JID.004.10xGY(9?5)3.jpeg	4.84E-05	-5.473	0.09	90
JID.004.10xGY(9?5)3.jpeg	3.67E-05	-5.44	0.068	68
JID.004.10xGY(9?5)3.jpeg	2.61E-05	-3.814	0.048	48
JID.004.10xGY(9?5)3.jpeg	3.58E-05	-4.151	0.066	66
JID.004.10xGY(9?5)3.jpeg	4.87E-05	-8.514	0.09	90
JID.004.10xGY(9?5)3.jpeg	3.32E-05	-14.158	0.061	61
JID.004.10xGY(9?5)3.jpeg	4.58E-05	-6.857	0.085	85
JID.004.10xGY(9?5)3.jpeg	4.12E-05	-5.231	0.076	76
JID.004.10xGY(9?5)3.jpeg	4.64E-05	-4.616	0.086	86

JID.004.10xGY(9?5)3.jpeg	4.12E-05	-5.988	0.077	77
JID.004.10xGY(9?5)3.jpeg	4.47E-05	0	0.083	83
JID.004.10xGY(9?5)3.jpeg	2.95E-05	-1.685	0.055	55
JID.004.10xGY(9?5)3.jpeg	2.29E-05	-11.739	0.042	42
JID.004.20xGY(9?5)6.jpeg	8.86E-06	0	0.032	32
JID.004.20xGY(9?5)6.jpeg	9.95E-06	-1.264	0.037	37
JID.004.20xGY(9?5)6.jpeg	8.06E-06	-17.942	0.03	30
JID.004.20xGY(9?5)6.jpeg	8.43E-06	-6.009	0.031	31
JID.004.20xGY(9?5)6.jpeg	1.22E-05	0	0.045	45
JID.004.20xGY(9?5)6.jpeg	8.35E-06	0	0.031	31
JID.004.20xGY(9?5)6.jpeg	7.12E-06	-16.756	0.026	26
JID.004.20xGY(9?5)6.jpeg	4.65E-06	-8.393	0.017	17
JID.004.40xGY(9?5)5.jpeg	1.24E-05	-15.141	0.094	94
JID.004.40xGY(9?5)5.jpeg	1.06E-05	-5.644	0.08	80
JID.004.40xGY(9?5)5.jpeg	9.56E-06	-6.153	0.072	72
JID.004.40xGY(9?5)5.jpeg	5.75E-06	-8.155	0.043	43
JID.004.40xGY(9?5)5.jpeg	7.16E-06	-10.115	0.054	54
JID.004.40xGY(9?5)5.jpeg	4.08E-06	-10.773	0.031	31
JID.005.10xGY2.jpeg	2.95E-05	-1.685	0.055	55
JID.005.10xGY2.jpeg	5.56E-05	-6.537	0.103	103
JID.005.10xGY2.jpeg	4.73E-05	-11.997	0.088	88
JID.005.10xGY2.jpeg	3.01E-05	-11.634	0.056	56
JID.005.10xGY2.jpeg	2.52E-05	-5.974	0.047	47
JID.005.10xGY2.jpeg	3.41E-05	-5.807	0.063	63
JID.005.10xGY2.jpeg	2.61E-05	-5.711	0.048	48
JID.005.10xGY2.jpeg	2.72E-05	-7.958	0.05	50
JID.005.10xGY2.jpeg	3.49E-05	-4.254	0.065	65
JID.005.10xGY1.jpeg	3.02E-05	-10.008	0.056	56
JID.005.10xGY1.jpeg	3.10E-05	-10.257	0.057	57
JID.005.10xGY1.jpeg	2.64E-05	-9.567	0.049	49
JID.005.10xGY1.jpeg	3.16E-05	-5.29	0.058	58
JID.005.10xGY1.jpeg	2.96E-05	-3.366	0.055	55
JID.005.10xGY1.jpeg	2.44E-05	-8.797	0.045	45
JID.005.10xGY1.jpeg	1.93E-05	-7.883	0.035	35

JID.005.10xGY1.jpeg	3.59E-05	-14.485	0.067	67
JID.005.10xGY1.jpeg	2.21E-05	-14.4	0.041	41
JID.005.10xGY1.jpeg	1.81E-05	-5.528	0.033	33
JID.005.10xGY1.jpeg	2.93E-05	-10.305	0.054	54
JID.005.10xGY1.jpeg	2.79E-05	-5.356	0.052	52
JID.005.10xGY1.jpeg	2.18E-05	-6.934	0.04	40
JID.005.10xGY1.jpeg	2.01E-05	-7.539	0.037	37
JID.005.10xGY1.jpeg	2.16E-05	0	0.04	40
JID.005.10xGY1.jpeg	1.41E-05	-15.461	0.026	26
JID.006.20xGY3.jpeg	9.81E-06	-7.707	0.036	36
JID.006.20xGY3.jpeg	1.32E-05	-4.79	0.049	49
JID.006.20xGY3.jpeg	6.90E-06	-7.352	0.025	25
JID.006.20xGY3.jpeg	5.96E-06	-4.289	0.022	22
JID.006.20xGY3.jpeg	1.01E-05	-9.189	0.037	37
JID.006.20xGY3.jpeg	1.22E-05	-10.768	0.045	45
JID.006.20xGY3.jpeg	6.18E-06	-16.699	0.023	23
JID.006.20xGY3.jpeg	7.85E-06	-10.257	0.029	29
JID.006.20xGY3.jpeg	6.68E-06	-7.595	0.024	24
JID.006.20xGY3.jpeg	6.39E-06	-23.025	0.024	24
JID.006.20xGY3.jpeg	8.14E-06	0	0.03	30
JID.006.20xGY3.jpeg	7.56E-06	-7.263	0.028	28
JID.006.20xGY3.jpeg	8.43E-06	-4.475	0.031	31
JID.005.20xGY2.jpeg	2.35E-05	-8.733	0.087	87
JID.005.20xGY2.jpeg	1.65E-05	-3.797	0.061	61
JID.005.20xGY2.jpeg	1.24E-05	-15.668	0.046	46
JID.005.20xGY2.jpeg	1.27E-05	-16.668	0.047	47
JID.005.20xGY2.jpeg	9.01E-06	-11.768	0.033	33
JID.005.20xGY2.jpeg	8.50E-06	-15.604	0.031	31
JID.005.20xGY2.jpeg	1.24E-05	-15.668	0.046	46
JID.005.20xGY1.jpeg	1.66E-05	-11.211	0.061	61
JID.005.20xGY1.jpeg	1.78E-05	-18.435	0.066	66
JID.005.20xGY1.jpeg	1.46E-05	-15.985	0.054	54
JID.005.20xGY1.jpeg	1.18E-05	-11.101	0.043	43
JID.005.20xGY1.jpeg	9.44E-06	-11.136	0.035	35

JID.005.20xGY1.jpeg	1.48E-05	-18.703	0.055	55
JID.005.20xGY1.jpeg	1.52E-05	-11.364	0.056	56
JID.005.20xGY1.jpeg	1.53E-05	-10.134	0.057	57
JID.005.20xGY2.jpeg	1.65E-05	-2.291	0.061	61
JID.005.20xGY2.jpeg	2.38E-05	-4.399	0.088	88
JID.005.20xGY2.jpeg	1.17E-05	-10.049	0.043	43
JID.005.20xGY2.jpeg	1.28E-05	-14.195	0.047	47
JID.005.20xGY2.jpeg	1.17E-05	-14.56	0.043	43
JID.005.20xGY2.jpeg	1.08E-05	-8.627	0.04	40
JID.005.20xGY2.jpeg	9.52E-06	-4.399	0.035	35
JID.005.20xGY2.jpeg	1.03E-05	-10.196	0.038	38
JID.006.20xGY1.jpeg	5.81E-06	-12.995	0.021	21
JID.006.20xGY1.jpeg	5.30E-06	-10.376	0.019	19
JID.006.20xGY1.jpeg	3.20E-06	0	0.012	12
JID.006.20xGY1.jpeg	5.30E-06	-7.224	0.019	19
JID.006.20xGY1.jpeg	5.38E-06	-14.783	0.02	20
JID.006.20xGY1.jpeg	8.35E-06	-12.2	0.031	31
JID.006.20xGY1.jpeg	5.23E-06	-4.83	0.019	19
JID.006.20xGY1.jpeg	6.39E-06	-27.15	0.023	23
JID.006.20xGY1.jpeg	6.83E-06	-3.691	0.025	25
JID.006.20xGY1.jpeg	9.08E-06	-5.985	0.033	33
JID.006.20xGY1.jpeg	6.03E-06	-12.68	0.022	22
JID.006.20xGY2.jpeg	7.34E-06	-16.26	0.027	27
JID.006.20xGY2.jpeg	7.70E-06	-13.772	0.028	28
JID.006.20xGY2.jpeg	1.04E-05	0	0.038	38
JID.006.20xGY2.jpeg	1.26E-05	-8.366	0.046	46
JID.006.20xGY2.jpeg	6.90E-06	-7.352	0.025	25
JID.006.20xGY2.jpeg	4.87E-06	-7.883	0.018	18
JID.006.20xGY2.jpeg	6.83E-06	-1.848	0.025	25
JID.006.20xGY2.jpeg	6.39E-06	-6.557	0.023	23
JID.006.20xGY2.jpeg	7.99E-06	-6.282	0.029	29
JID.006.20xGY2.jpeg	8.72E-06	8.673	0.032	32
JID.006.20xGY2.jpeg	8.94E-06	-7.595	0.033	33
JID.006.20xGY2.jpeg	5.52E-06	-9.964	0.02	20

JID.006.20xGY2.jpeg	5.09E-06	-10.67	0.019	19
JID.006.20xGY2.jpeg	6.39E-06	-7.943	0.024	24
JID.006.20xGY2.jpeg	7.85E-06	-11.725	0.029	29
JID.006.20xGY2.jpeg	7.19E-06	-11.195	0.026	26
JID.006.20xGY2.jpeg	8.21E-06	-4.635	0.03	30
JID.006.20xGY2.jpeg	7.05E-06	-3.576	0.026	26
JID.006.20xGY2.jpeg	1.45E-05	-9.891	0.053	53
JID.006.20xGY2.jpeg	9.74E-06	-2.583	0.036	36
JID.006.20xGY2.jpeg	7.19E-06	-11.31	0.026	26
JID.006.20xGY2.jpeg	1.07E-05	-6.254	0.039	39
JID.006.20xGY2.jpeg	1.32E-05	-2.878	0.048	48
JID.006.20xGY2.jpeg	7.05E-06	-3.576	0.026	26
JID.006.20xGY2.jpeg	6.18E-06	-6.789	0.023	23
JID.006.20xGY2.jpeg	6.61E-06	-6.411	0.024	24
JID.006.20xGY2.jpeg	5.67E-06	0	0.021	21
JID.006.20xGY2.jpeg	7.05E-06	-1.79	0.026	26
JID.006.20xGY2.jpeg	7.99E-06	6.282	0.029	29
JID.006.20xGY2.jpeg	6.39E-06	-5.906	0.023	23
JID.006.20xGY2.jpeg	7.27E-06	5.768	0.027	27
JID.006.20xGY2.jpeg	5.52E-06	-9.964	0.02	20
JID.006.20xGY2.jpeg	8.72E-06	-7.722	0.032	32
JID.006.20xGY2.jpeg	6.32E-06	-12.236	0.023	23
JID.006.20xGY2.jpeg	5.45E-06	-2.322	0.02	20
JID.006.20xGY2.jpeg	6.68E-06	-8.219	0.024	24
JID.006.20xGY2.jpeg	7.77E-06	-8.13	0.029	29
JID.006.20xGY2.jpeg	7.12E-06	-7.792	0.026	26
JID.006.20xGY2.jpeg	9.74E-06	2.583	0.036	36
JID.006.20xGY2.jpeg	8.72E-06	-6.766	0.032	32
JID.006.20xGY2.jpeg	6.61E-06	-5.711	0.024	24
JID.006.20xGY2.jpeg	1.04E-05	-1.614	0.038	38
JID.006.20xGY2.jpeg	1.41E-05	-7.125	0.052	52
JID.006.20xGY2.jpeg	1.18E-05	0	0.043	43
JID.006.20xGY2.jpeg	7.48E-06	0	0.028	28
JID.006.20xGY2.jpeg	5.52E-06	-6.934	0.02	20

JID.006.40xGY2.jpeg	2.66E-06	-9.15	0.02	20
JID.006.40xGY2.jpeg	3.33E-06	-8.303	0.025	25
JID.006.40xGY2.jpeg	4.48E-06	-8.643	0.034	34
JID.006.40xGY2.jpeg	3.35E-06	-11.547	0.025	25
JID.006.40xGY2.jpeg	3.03E-06	-12.492	0.023	23
JID.006.40xGY2.jpeg	3.95E-06	-4.87	0.03	30
JID.006.40xGY2.jpeg	3.62E-06	-10.43	0.027	27
JID.006.40xGY2.jpeg	4.39E-06	-13.756	0.033	33
JID.011.20xGY(9?5).jpeg	9.01E-06	-9.846	0.033	33
JID.011.20xGY(9?5).jpeg	1.45E-05	-4.62	0.053	53
JID.011.20xGY(9?5).jpeg	8.94E-06	-7.067	0.033	33
JID.011.20xGY(9?5).jpeg	6.32E-06	-14.676	0.023	23
JID.011.20xGY(9?5).jpeg	8.50E-06	-9.462	0.031	31
JID.011.20xGY(9?5).jpeg	1.01E-05	-9.189	0.037	37
JID.011.20xGY(9?5).jpeg	1.22E-05	-11.712	0.045	45
JID.011.20xGY(9?5).jpeg	1.71E-05	-13.505	0.063	63
JID.006.20xGY3.jpeg	1.27E-05	-4.955	0.047	47
JID.006.20xGY3.jpeg	1.18E-05	-11.17	0.043	43
JID.006.20xGY3.jpeg	1.14E-05	-14.125	0.042	42
JID.006.20xGY3.jpeg	9.23E-06	-11.489	0.034	34
JID.006.20xGY3.jpeg	6.68E-06	-17.241	0.025	25
JID.006.20xGY3.jpeg	5.30E-06	-7.224	0.019	19
JID.006.20xGY3.jpeg	8.21E-06	-8.13	0.03	30
JID.006.20xGY3.jpeg	6.39E-06	-7.853	0.024	24
JID.006.20xGY3.jpeg	7.70E-06	-3.778	0.028	28
JID.006.20xGY3.jpeg	6.54E-06	-13.722	0.024	24
JID.006.20xGY3.jpeg	5.01E-06	-5.042	0.018	18
JID.006.20xGY3.jpeg	8.57E-06	0	0.032	32
JID.006.20xGY3.jpeg	6.18E-06	-17.152	0.023	23
JID.011.20xGY(9?7).jpeg	1.40E-05	-10.198	0.052	52
JID.011.20xGY(9?7).jpeg	1.76E-05	-12.709	0.065	65
JID.011.20xGY(9?7).jpeg	1.02E-05	-7.729	0.038	38
JID.011.20xGY(9?7).jpeg	9.52E-06	-12.433	0.035	35
JID.011.20xGY(9?7).jpeg	1.45E-05	-7.196	0.054	54

JID.011.20xGY(9?7).jpeg	1.02E-05	-4.934	0.038	38
JID.011.20xGY(9?7).jpeg	1.11E-05	-11.753	0.041	41
JID.011.20xGY(9?7).jpeg	1.23E-05	-12.714	0.045	45

VITA

Jeremy Dunham is from Stone Mountain, GA. He completed his AA at Georgia Perimeter College, and later completed his BS in Geology at Georgia state University with a focus on geochemistry before making his way to The University of Tennessee. His future plans include either pursuing a career in geochemistry related to exploration mining geochemistry and/or biogeochemistry related to environmental remediation, or work at a national laboratory in geology.